OFFICE OF NAVAL RESEARCH

Contract N00014-82-0280

Task No. NR413EOOl

TECHNICAL REPORT NO. 52

Chlorine Bonding Sites and Bonding Configurations on Si(100)-(2x1)

by

Q. Gao, C.C. Cheng, P.J. Chen, W.J. Choyke and J.T. Yates, Jr.

Submitted To

Journal of Chemical Physics

Surface Science Center
Department of Chemistry
University of Pittsburgh
Pittsburgh, PA 15260

September 16, 1992

UNCLASSIFIED
SECURITY CLASSIFICATION OF THIS PAGE (When Data Entered)

MASTER COPY - FOR REPRODUCTION PURPOSES

REPORT DOCUMENTATION PAGE

READ INSTRUCTIONS BEFORE COMPLETING FORM

1. REPORT NUMBER: 52

2. GOVT ACCESSION NO.

3. RECIPIENT'S CATALOG NUMBER

4. TITLE (and Subtitle): Chlorine Bonding Sites and Bonding Configurations on Si(100)-(2x1)

5. TYPE OF REPORT & PERIOD COVERED: Preprint

6. PERFORMING ORG. REPORT NUMBER

7. AUTHOR(s): Q. Gao, C.C. Cheng, P.J. Chen, W.J. Choyke and J.T. Yates, Jr.

8. CONTRACT OR GRANT NUMBER(s)

9. PERFORMING ORGANIZATION NAME AND ADDRESS: Surface Science Center, Department of Chemistry, University of Pittsburgh, Pittsburgh, PA 15260

10. PROGRAM ELEMENT, PROJECT, TASK AREA & WORK UNIT NUMBERS

11. CONTROLLING OFFICE NAME AND ADDRESS

12. REPORT DATE: 16 September 1992

13. NUMBER OF PAGES

14. MONITORING AGENCY NAME & ADDRESS (if different from Controlling Office)

15. SECURITY CLASS. (of this report): Unclassified

15a. DECLASSIFICATION/DOWNGRADING SCHEDULE

16. DISTRIBUTION STATEMENT (of this Report)

17. DISTRIBUTION STATEMENT (of the abstract entered in Block 20, if different from Report)

18. SUPPLEMENTARY NOTES

19. KEY WORDS (Continue on reverse side if necessary and identify by block number)

silicon
chlorine
ESDIAD
etching
Si(100)

20. ABSTRACT (Continue on reverse side if necessary and identify

A combination of experimental methods has been employed for the study of Cl_2 adsorption and reaction on Si(100)-(2x1). At 100K, Cl_2 adsorption occurs rapidly to a coverage of ~0.7 Cl/Si. This is followed by slower adsorption kinetics with further Cl_2 exposure. Two Cl adsorption states are observed experimentally. One of the adsorption states is terminally bonded Cl on the inclined dangling bond of the symmetric Si_2 dimer sites, with vibrational frequency, $\nu(SiCl)$ of 590 ± 600 cm^{-1}. These bonded Cl atoms give four off-normal Cl^+ ESDIAD emission beams from the orthogonal domains of silicon dimer sites. The Si Cl bond angle for this adsorption configuration is estimated to be inclined 25°±4° off normal. The second Cl adsorption state, a minority species, is bridge bonded Cl with $\nu(Si_2Cl_2)$ of ~ 295 cm^{-1} which produces Cl^+ ion emission along the surface normal direction. Both adsorption states are present at low temperatures. Irreversible conversion from bridge bonded Cl to terminally bonded Cl begins to occur near 300K; the conversion is complete near ~673K. LEED studies indicate that the (2x1) reconstruction for the substrate is preserved for all Cl coverages.

The most probable Cl^+ kinetic energy in electron stimulated desorption (ESD) is 1.1 $^{+0.5}_{-0.3}$ eV. A significant adsorbate adsorbate quenching effect reducing the Cl^+ ion yield in ESD occurs above a Cl(a) coverage of ~0.5 ML (monolayer) due to interadsorbate interactions. The maximum Cl^+ yield is about 4×10^{-2} Cl^+ e at an electron energy of 120 eV.

Temperature programmed desorption results show that $SiCl_2$ is the major etching product which desorbs at about 840K.

tered)

DD FORM 1 JAN 73 1473 EDITION OF 1 NOV 65 IS OBSOLETE

Submitted to: Journal of Chemical Physics

Date: September 16, 1992

Chlorine Bonding Sites and Bonding Configurations on Si(100)-(2x1)

Q. Gao, C. C. Cheng, P. J. Chen*, W. J. Choyke* and J. T. Yates, Jr.

Surface Science Center
Department of Chemistry
University of Pittsburgh
Pittsburgh, PA 15260

*Department of Physics
University of Pittsburgh
Pittsburgh, PA 15260

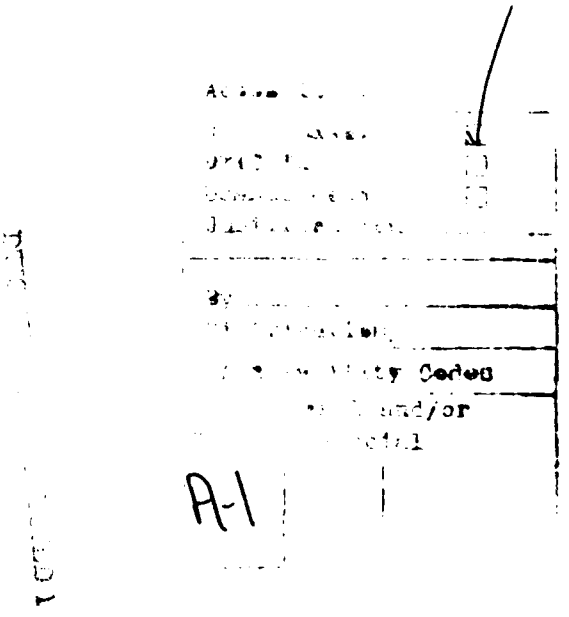

Chlorine Bonding Sites and Bonding Configurations on Si(100)-(2x1)

Q. Gao, C. C. Cheng, P. J. Chen*, W. J. Choyke* and J. T. Yates, Jr.

Surface Science Center
Department of Chemistry
University of Pittsburgh
Pittsburgh, PA 15260

*Department of Physics
University of Pittsburgh
Pittsburgh, PA 15260

Abstract

A combination of experimental methods has been employed for the study of Cl_2 adsorption and reaction on Si(100)-(2x1). At 100K, Cl_2 adsorption occurs rapidly to a coverage of ~0.7 Cl/Si. This is followed by slower adsorption kinetics with further Cl_2 exposure. Two Cl adsorption states are observed experimentally. One of the adsorption states is terminally bonded Cl on the inclined dangling bond of the symmetric Si_2 dimer sites, with vibrational frequency, ν(SiCl) of 550 ~ 600 cm^{-1}. These bonded Cl atoms give four off-normal Cl^+ ESDIAD emission beams from the orthogonal domains of silicon dimer sites. The Si-Cl bond angle for this adsorption configuration is estimated to be inclined 25°±4° off-normal. The second Cl adsorption state, a minority species, is bridge bonded Cl with $\nu(Si_2Cl)$ of ~ 295 cm^{-1} which produces Cl^+ ion emission along the surface normal direction. Both adsorption states are present at low temperatures. Irreversible conversion from bridge bonded Cl to terminally bonded Cl begins to occur near 300K; the conversion is complete near ~673K. LEED studies indicate that the (2x1) reconstruction for the substrate is

preserved for all Cl coverages.

The most probable Cl^+ kinetic energy in electron stimulated desorption, ESD, is $1.1^{+\ 0.6}_{-\ 0.3}$ eV. A significant adsorbate-adsorbate quenching effect reducing the Cl^+ ion yield in ESD occurs above a Cl(a) coverage of ~0.5 ML (monolayer) due to interadsorbate interactions. The maximum Cl^+ yield is about $4x10^{-7}$ Cl^+/e at an electron energy of 120 eV.

Temperature programmed desorption results show that $SiCl_2$ is the major etching product which desorbs at about 840K.

1. Introduction

The chemisorption of chlorine on silicon is of importance since the interaction between Si and Cl plays an essential role in VLSI technologies such as dry etching, photo surface cleaning, and Si epitaxial growth [1-5]. An understanding of the bonding structure and stability of chemisorbed chlorine on the Si(100) surface is necessary for a complete description of the surface reactions in the etching and epitaxial growth processes.

The chemisorption of chlorine on Si(100) surface has been studied using a wide variety of surface science techniques [6-12]. However, fundamental issues concerning the Si-Cl bond, such as the Cl bonding configuration and Cl binding sites, are still not well understood. Controversial conclusions are reported in the literature. For example, UV photoemission studies of Cl_2 adsorption on Si(100)-(2x1) at room temperature [6] indicate that Si-Cl bonds are covalent in character and tilted with respect to the surface normal. However, recent studies of chlorine adsorption on Si(100)-(2x1) at ~500K [7-8], using a vicinal single domain surface, conclude that the Si-Cl bond is perpendicular to the (100) surface (within 10°) based on the polarization-dependence of the Cl(a) K-edge NEXAFS (near-edge x-ray absorption fine structure) measurements. This disagrees with the previous tilted Si-Cl bond model. This perpendicular bonding geometry is proposed to result from atop bonding of Cl on a buckled (asymmetric) dimer with a Si-Cl bond length of ~2.00 Å.

Earlier measurements involving surface polarization-dependent near-edge x-ray absorption fine structure (NEXAFS) at the Cl(a) K-edge [9] indicated that the Si-Cl bond length is ~1.95 Å, with the Si-Cl bond tilted ~25° off-normal. Since the scanning tunneling microscopy (STM) data show a mixture of symmetric and asymmetric Si-Si dimers on the clean Si(100)-(2x1) surface [13], an adsorption model was invoked where

chlorine adsorption would convert the asymmetric dimer structure to the symmetric dimer structure [14]. Polarization-dependent angle-resolved photoemission studies [10] for chlorine adsorption (at 473K substrate temperature to prevent the weakly bound chlorine phase formation [11]) on a single domain Si(100)-(2x1) surface indicate the presence of mirror-plane symmetry. This is consistent with an adsorption model where two Cl atoms adsorb on each of the inclined dangling bonds of the symmetric Si_2 dimer.

Low energy electron diffraction (LEED) results for saturation chlorine exposures confirm the (2x1) reconstruction for the Cl/Si(100) system [6] indicating that the Si-Si dimer bond is preserved after chlorine adsorption. Low energy electron loss spectroscopy (LEELS) studies [12] reveal that an electronic transition occurs at ~8.8 eV for Si-Cl σ bonding which is related to the Cl(p_z) state. Another electronic transition occurs at ~7.2 eV for π-like bonding which is related to the Cl(p_x, p_y) states. Binding sites associated with these electronic transitions are assigned to the surface dangling bonds at step edges and at defect sites, or on the Si dimers.

The digital ESDIAD (electron stimulated desorption ion angular distribution) method is a powerful technique for the measurement of chemical bond orientations with high precision (~1°). This capability has been demonstrated repeatedly since its invention [15-16]. High resolution electron energy loss spectroscopy (HREELS) provides surface species identification through vibrational characterization. The combination of these two measurement techniques together with other surface analysis methods provide new information about the local structure and chemical bonding of Cl on the Si(100)-(2x1) surface.

In this report we present direct evidence from digital ESDIAD and HREELS for the presence of both bridged Cl bonding as well as tilted bonding of Cl on the Si(100)

surface. The bridged Cl species are postulated to be bonded symmetrically between Si dimer atoms; the tilted Cl species are bound to inclined Si dangling bonds at the ends of the Si dimer atoms. In addition, conditions are determined for causing thermally activated conversion from one bonding configuration to the other configuration. These findings help to resolve the controversy about two different Cl bonding configurations.

2. Experimental

The ultrahigh vacuum chamber employed for digital ESDIAD/LEED and temperature programmed desorption (TPD) has a base pressure of ~3×10^{-11} Torr. A detailed description of the digital ESDIAD/LEED system can be found elsewhere [17]. Basically, it is equipped with a CMA Auger electron spectrometer (AES), an argon sputtering gun, a digital ESDIAD/LEED apparatus, a shielded quadrupole mass spectrometer (QMS) for line-of-sight TPD studies, and an additional QMS with an electron gun and grid lenses for ion mass analysis during electron stimulated desorption (ESD).

The digital ESDIAD/LEED apparatus (the reader is referred to fig. 15 for a diagram) contains an electron gun providing a ~1 mm diameter electron beam impinging onto the crystal. The electron beam energy used for the ESDIAD studies is 120 eV. The grids and crystal are biased with respect to ground as follows: $V_{G_1} = V_{G_2} = V_{G_3} = 0$ V, $V_{G_4} = V_{crystal} = +10$ V, $V_{G_5} = -500$ V where G_1 is the hemispherical grid closest to the crystal and G_5 is a planar grid in front of the microchannel plate (MCP) detector. A structureless background ESDIAD pattern was obtained with $V_{G_4} = +13$ V (sufficient to retard all desorbed positive ions). This background (thought to be due mainly to soft x-rays [18]) is then used for subsequent digital background subtraction. All ESDIAD data are collected at a crystal temperature of 120K. A two fold symmetrization smoothing procedure [19] was employed for the

ESDIAD patterns shown in this paper to remove the slight inhomogeneous response of the ion optics and/or the MCP detector. The selection of two fold symmetry is based on the symmetry observed in the ESDIAD pattern and the assumption of an equal statistical population of Cl atoms adsorbed on the dangling bonds of the Si_2 dimer sites at the opposite polar angles with respect to the surface normal.

The Si (100)-(2x1) crystal (Czochralski grown, 10 Ω cm, p-type, B-doped) was cleaned by Ar^+ bombardment followed by annealing to 1200K and slowly cooling. AES indicates a clean surface with C(KLL):Si(LMM), O(KLL):Si(LMM), Cl(LMM):Si(LMM) AES peak-to-peak intensity ratios $< 1x10^{-3}$. The surface reconstruction was checked with LEED which clearly indicated both (2x1) and (1x2) diffraction spots. Cl_2 gas was purchased from Matheson with high purity (>99.5%). Further purification of the Cl_2 gas by freeze-pump-thaw cycles was performed before use. The dosing gas line was well conditioned with Cl_2 gas. A multicapillary-collimated doser [20] was used for Cl_2 exposures. The dosing flux was calibrated with pressure drop measurements, using $N_2(g)$, in the gas handling system with appropriate correction for the molecular mass difference. In addition, for the flux correction, proper consideration was made for the crystal and the doser geometry [21]. The crystal temperature was carefully monitored with a chromel-constantan (type-E) thermocouple enclosed in a small double Ta-foil envelope inserted into a slot in the crystal edge. Mass spectroscopic studies of the ions produced from the Cl/Si(100) surface indicate that Cl^+ ions are the species contributing to the observed ESDIAD pattern.

A second UHV chamber with a base pressure of $\sim 1x10^{-10}$ mbar housed a Leybold-Heraeus ELS-22 high resolution electron energy loss spectrometer (HREELS) for vibrational analysis, a shielded QMS for line-of-sight TPD studies, a CMA-AES, a sputtering gun, a microchannel plate LEED apparatus and a calibrated multicapillary-collimated doser. A detailed description of the chamber was given previously [22]. For

HREELS studies a primary beam energy of 4.2 eV was used. A full-width-at-half-maximum (FWHM) of 65 cm^{-1} for the elastic beam was routinely obtained. Cross comparison of the Cl_2 exposure was obtained from the break point of the adsorption kinetics measured in the two chambers.

3. Results

3.1 AES Study of Cl_2 Adsorption on Si(100)-(2x1)

Due to the presence of the ESD effect for Cl(a) species during the AES data collection time interval, special care was taken to minimize its influence on the accuracy and reproducibility of the Cl uptake measurement. This includes scanning the Cl (LMM) transition at 181 eV first, then scanning the Si (LMM) transition at 92 eV while keeping the scanning time as short as possible. Furthermore, several probing points on the crystal were used and the AES intensities were averaged. The AES uptake measurement for Cl_2 adsorption on Si(100)-(2x1) crystal at 100K is shown in fig. 1. The Cl/Si peak-to-peak intensity ratio exhibits an initial linear increase as a function of Cl_2 exposure. Beyond an exposure of ~ $2.4x10^{14}$ molecules/cm^2, the Cl_2 adsorption rate is significantly reduced. The linear fitting for the AES uptake curve in the two adsorption rate regions gives a break point at an exposure of ~$2.4x10^{14}$ Cl_2/cm^2.

3.2 Thermal Desorption Studies Following Cl_2 Adsorption on Si(100)-(2x1)

Temperature programmed desorption for various Cl_2 exposures on Si(100)-(2x1) at 120K were measured. The following possible products were monitored: Cl_2 (m/e=70 amu for Cl_2^+, and m/e=35 amu for Cl^+); $SiCl_2$ (m/e=98 amu for $SiCl_2^+$ and m/e=63 amu for $SiCl^+$); and $SiCl_4$ (m/e=168 amu for $SiCl_4^+$, m/e=133 amu

for $SiCl_3^+$, and m/e=63 amu for $SiCl^+$). At all Cl_2 exposures, no Cl_2 desorption was detected. $SiCl_2$ was the only desorption product for Cl_2 exposures below $2.4x10^{14}$ molecules/cm^2. Beyond this exposure, a small amount of $SiCl_4$ desorption was also detected.

Figure 2 shows the TPD results. At a Cl_2 exposure of $0.5x10^{14}$ molecules/cm^2 (fig. 2a), $SiCl_2$ desorption was observed with a peak temperature of 848K (monitored with its major fragment, $SiCl^+$, m/e=63 amu). For a Cl_2 exposure of $1.0x10^{14}$ molecules/cm^2, the $SiCl_2$ desorption peak shifted downward to 837K (fig. 2b). At a Cl_2 exposure of $2.6x10^{14}$ molecules/cm^2, the $SiCl_2$ desorption peak shifted further downward to 825K (fig. 2c). In addition, a very small amount of $SiCl_4$ of desorption was observed at ~500K (identified with its major mass spectrometer fragment, $SiCl_3^+$, m/e=133 amu). For a high Cl_2 exposure of $4.6x10^{14}$ molecules/cm^2, the low temperature $SiCl_4$ desorption peak is more pronounced (fig. 2d and the insert in the figure).

Since Cl_2 is not a thermal desorption product at any coverage, the amount of silicon chlorides desorbed is a direct indication of the quantity of surface chlorine present. Fig. 3 is a plot of the yield of $SiCl^+$ from $SiCl_2$ (T_p ~ 840K) and $SiCl_4$ (T_p ~ 500K) desorption versus Cl_2 exposure. It is evident that at ~$2.4x10^{14}$ Cl_2/cm^2 exposure, the rate of Cl_2 adsorption has decreased significantly as judged from the break in the $SiCl_2$ yield curve. This is consistent with the break point in the AES uptake curve (fig.1). Beyond this exposure, a small amount of the higher chloride, $SiCl_4$, was produced as well.

3.3 LEED Study of Cl_2 Adsorption on Si(100)-(2x1)

In order to understand the effect of Cl_2 adsorption on the long range ordering of the Si(100)-(2x1) substrate, we have employed digital LEED to study the intensity

ratios for the half-order diffraction peak versus the first-order diffraction peak as a function of Cl_2 exposure. The results are shown in fig. 4 where average intensity ratios measured in (1/2,0),(1,0), (0,1/2) and (0,1) beams are used for the (2x1) and (1x2) domains. The half-order diffraction was preserved for all Cl_2 exposures. Additionally, a monotor ic decrease of the intensity ratio was observed for the half-order diffraction beam versus the first-order diffraction beam for Cl_2 exposures less than ~$2.4x10^{14}$ molecules/cm^2. Further Cl_2 exposure beyond this point results in a nearly constant LEED intensity ratio for the half-order diffraction vs. the first-order diffraction.

3.4 Digital ESDIAD Study of Cl_2 Adsorption on Si(100)-(2x1)

3.4.1 Coverage Dependent ESDIAD Study

ESDIAD results for chlorine chemisorbed on Si(100)-(2x1) at 120K are shown in fig. 5. At a Cl_2 exposure of $0.5x10^{14}$ molecules/cm^2 (fig. 5a), the ESDIAD pattern consists of a broad Cl^+ ion emission beam directed along the surface normal with shoulders along the [011] and [01$\bar{1}$] directions across the center. The contour diagrams at several chlorine coverages (fig. 5a-c) indicate the presence of four orthogonally directed shoulders corresponding to the (1x2) and (2x1) domains of the substrate. As the Cl_2 exposure was increased to $1.3x10^{14}$ molecules/cm^2, the Cl^+ ion yield increased and the ESDIAD pattern retained identical shape and symmetry (fig. 5b). At a Cl_2 exposure of $2.6x10^{14}$ molecules/cm^2, the Cl^+ ion yield decreased but the ESDIAD pattern retained of similar shape with slightly stronger evidence of the shoulder features.

After annealing each of the above Si(100)-(2x1) surfaces containing various coverages of chlorine to 673K , a temperature where no thermal desorption occurs at submonolayer coverage, a dramatic ESDIAD pattern change was observed. As a

function of initial Cl_2 exposure, the ESDIAD patterns of the annealed Cl/Si(100) surface are shown in fig. 6. It is clear that at all chlorine initial coverages, the 673K annealing changed the original ESDIAD pattern into a pattern containing four well separated off-normal Cl^+ beams oriented in azimuth along the [011] and [01$\bar{1}$] directions. Additionally, the cross sectioned contours at different peak heights for each of these four beams are essentially circular.

3.4.2 Detailed Temperature Dependent ESDIAD Study

Details of ESDIAD pattern development for Cl_2/Si(100)-(2x1) as a function of annealing temperature are shown in fig. 7 (Cl_2 exposure ~2.4×10^{14} molecules/cm^2). Cl_2 adsorption at 120K led to a broad centered ESDIAD pattern containing four shoulders (fig. 7a) just as that shown in fig. 5c. Annealing the crystal to 273K gave a similar ESDIAD pattern (fig.7b) with four enhanced shoulder peaks. Annealing the crystal to 423K leads to a considerable decrease of the intensity ratio for the normal-emission ion beam relative to that of the four off-normal ion emission beams (previous shoulder peaks) as shown in fig.7c. This conversion from normal beam to off-normal beams appears to begin near 300K [23]. The development of the four off-normal Cl^+ beams is more evident after annealing the crystal to 523K (fig.7d). A completely developed four-beam ESDIAD pattern is observed after annealing the crystal to 673K (fig.7e). At this annealing temperature, the normal emission Cl^+ ion beam has almost completely disappeared. Further annealing to 823K (fig. 7f) causes considerable etching of the substrate, producing $SiCl_2(g)$, as can be seen from the TPD results (fig. 2). The ESDIAD pattern following 823K annealing shows a centered beam with a pair of orthogonal two fold symmetric contours. The increase in Cl^+ ion yield (note fig. 7f, amplification factor 0.2) is due to a decrease of Cl(a) coverage as discussed in the next section.

Fig. 8 shows a cross section cut through the Cl^+ ESDIAD pattern along the [011] direction parallel to one of the Si_2 surface dimer bond directions. The loss of the normal Cl^+ beam during annealing, accompanied by the emergence of the off-normal Cl^+ beams, is clearly indicated. To avoid effects associated with a strong coverage dependent variation in Cl^+ ESD cross section, the cross-sectional patterns in fig. 8 were obtained from ESDIAD patterns normalized to contain the same number of Cl^+ ion counts.

3.5 The Characterization of Cl^+ Ions from Electron Stimulated Desorption

3.5.1 Cl^+ Ion Yield Measurements

The Cl^+ ion yield versus the Cl_2 exposure is plotted in fig. 9 for both the normal Cl^+ ion emission beam from low temperature Cl_2 adsorption and for the four off-normal Cl^+ ion emission beams obtained after annealing the Cl covered Si(100) crystal to 673K. For these measurements, the total number of counts within the ESDIAD pattern was obtained with a constant incident electron current. Initially it appears that the Cl^+ ion yield increases linearly with Cl_2 exposure to an intermediate Cl(a) coverage. Then, a decrease of Cl^+ ion yield is observed with further Cl_2 exposure.

3.5.2 Cl^+ Ion Energy Distribution Measurements

The kinetic energy distribution of Cl^+ ions was measured by retarding the Cl^+ ions with grid 4 positively biased relative to the potential on the crystal (the reader is referred to fig. 15). The result is shown in fig. 10. It is noticed that Cl^+ ions have very small kinetic energies with the most probable energy at ~0.3 eV (without correction for the work function difference between the crystal and the grids). The FWHM for the Cl^+ ion kinetic energy is about 0.6 eV. No difference is observed

within the resolution of our apparatus for the energy distributions of the normal Cl^+ ion beam (fig. 5) and the four off-normal Cl^+ ion beams (fig.6).

3.6 An Electron Beam Induced Desorption Study-High Electron Flux

In this experiment the chlorine covered Si(100) surface (exposure= $2x10^{14}$ Cl_2/cm^2) with a broad centered-peak ESDIAD pattern (fig. 11a) was subjected to a high electron flux using the diffuse stray electrons from the QMS ionization source (E_e = 170 eV;$I_{crystal}$ = 0.22 mA). After an exposure of ~$4.5x10^{18}$ electrons/cm^2 at a constant crystal temperature of 120K, we observed that the Cl^+ ion yield has decreased indicating a reduction of the Cl(a) coverage due to the electron stimulated desorption process. In addition, an ESDIAD pattern with a more significant contribution from the off-normal four-beam Cl^+ ion emission pattern is observed [fig. 11b], as the species responsible for the normal Cl^+ beam are preferentially depleted by the ESD process.

3.7 HREELS Study of Cl_2 Adsorption on Si(100)-(2x1)

3.7.1 Coverage Dependent HREELS Study

As a function of Cl_2 exposure, a series of HREELS measurements were carried out (fig. 12). After a Cl_2 exposure of $0.5x10^{14}$ molecules/cm^2 at 100K, a strong loss peak is observed at 553 cm^{-1} (fig 12a) which is assigned as the Si-Cl stretching mode, ν(SiCl) [24]. Weak peaks at ~800 cm^{-1}, ~900 cm^{-1} and 2100 cm^{-1} are also observed. It is well documented that the Si(100)-(2x1) surface is very active for H_2O dissociative adsorption, producing ν(SiH) at ~2100 cm^{-1}, and δ(OH) and ν(Si-OH) at ~800 cm^{-1} [25a-c]. Thus, we believe that very low levels of water contamination from the chamber background are responsible for these weak peaks. For a Cl_2 exposure of $2.2x10^{14}$ molecules/cm^2 (fig.12b), similar vibrational characteristics are observed. In

all spectra, a small vibrational loss feature in the range of 290~300 cm^{-1} is seen which becomes slightly more pronounced for higher Cl_2 exposures while shifting down in frequency (fig 12a-d). As will be discussed later, this peak can be assigned to the stretching mode for the bridge bonded Cl(a) species. A double loss or overtone of the ν(SiCl) mode can be seen at ~1190 cm^{-1}. The weak intensity of this peak is expected due to the small electron scattering cross-sections for multiple or overtone losses.

It should be emphasized that for all Cl_2 exposures, no surface di-, tri- or tetra-chlorides were observed from the HREELS analysis. Such higher chlorides would give an asymmetric as well as a symmetric Si-Cl stretching mode which would be expected at 533–616 cm^{-1} and 376–458 cm^{-1}, respectively [24]. In addition, a deformation mode is expected at 145–229 cm^{-1} [24]. With the resolution of our measurements, we would have observed the latter two modes if they were present with sufficient intensity. Furthermore, the Si-Cl stretching mode at ~ 600 cm^{-1} has nearly the same line width as the elastic peak. Thus, the high degree of homogeneity in the surface monochloride vibrational mode supports the conclusion that other higher chloride species are absent. The Si-Cl stretching mode is found to shift to higher frequencies as a function of Cl_2 exposure, which is an expected result for dipole-dipole interactions among the Si-Cl oscillators.

3.7.2 HREELS Study as a Function of Annealing Temperature

The temperature dependent HREELS results are shown in fig. 13. Adsorption of Cl_2 at 100K (exposure ~ 7.4×10^{14} Cl_2/cm^2) resulted in a strong ν(SiCl) stretching mode observed at ~600 cm^{-1} and a small loss peak observed at ~295 cm^{-1} (fig. 13a). Other low intensity vibrational features have been described and assigned in section 3.7.1. Annealing the Cl/Si(100)-(2x1) surface to 473K, where a four beam off-normal Cl^+ ESDIAD pattern was prominent, resulted in a slight intensity increase of the

ν(SiCl) peak at ~600 cm^{-1} and an intensity decrease of the weak peak at ~295 cm^{-1} (fig. 13b). Further annealing to 673K, a temperature corresponding to the completely developed four-beam ESDIAD pattern, resulted in further intensity reduction of the ~ 295 cm^{-1} peak (fig. 13c). Heating to 875K, a temperature where the etching reaction has occurred (fig.2), resulted in a decrease in the ν(SiCl) mode intensity and a slight shift of this mode to ~570 cm^{-1}. This analysis shows that the initial thermally induced disappearance of the Cl^+ ion emission along the surface normal direction observed in ESDIAD seems to be correlated with the disappearance of the vibrational peak at ~295 cm^{-1} and this will be discussed in detail below. In addition, the 875K etching of the substrate ($SiCl_2$ desorption) reduces the peak intensity of the ν(SiCl) mode at ~600 cm^{-1}.

4. Discussion

4.1 Monolayer Coverage of Chlorine

The adsorption of Cl_2 on Si(100)-(2x1) at ~100K has a relatively high adsorption rate initially which is directly proportional to the Cl_2(g) fluence, then undergoes a sudden reduction in adsorption rate as indicated by coverage sensitive studies using AES (fig.1), by quantitative TPD (fig.3) and by LEED measurements (fig.4). A dramatic decrease in Cl_2 adsorption rate is observed for the three measurements at a Cl_2 exposure above ~$2.4x10^{14}$ molecules/cm^2. The surface density of dangling bonds on Si(100)-(2x1) is $6.8x10^{14}$ /cm^2, assuming a perfect surface. The number of Cl atoms/cm^2 at the break point is ~$4.8x10^{14}$/cm^2, corresponding to ~70% of the number of dangling bonds available. Thus, one may conclude that repulsive interactions between Si-Cl species are probably responsible for the kinetic break. It is unlikely that 30% defect sites could exist on the Si(100) crystals [13]. As the Cl_2 exposure increases, the Cl coverage increases slowly to ~$5.8x10^{14}$ Cl/cm^2 in the

experiment at 100K.

4.2 Surface Species Present at 100K

It is evident that Cl_2 adsorption at 100K is dissociative for two reasons: (1) no Cl_2 molecular species are observed in HREELS. The molecular Cl_2 would give a Cl-Cl stretching mode near 546 cm^{-1} [26] which could be vibrationally excited at least by the impact scattering mechanism [27]; (2) no molecular Cl_2 desorption is observed in TPD experiments for all Cl_2 exposures.

The major surface species is identified as silicon monochloride based on the following arguments: (1) No higher surface silicon chlorides species such as di-, tri-, or tetrachloride are observed by HREELS. All these higher chlorides are expected to have a symmetric Si-Cl stretching mode, an asymmetric Si-Cl stretching mode, and Si-Cl deformation modes at 376~465 cm^{-1}, 533~617 cm^{-1} and 145~240 cm^{-1}, respectively [24]; In table 1, the vibrational modes of silicon mono-, di-, tri- and tetra-chlorides are listed, and a comparison is made to the surface chloride species observed in this study. (2) Our separate HREELS experiments for $SiCl_4$ adsorption on Si(100)-(2x1) clearly indicate that these modes are observable for higher chloride species [28]; (3) If the surface species is silicon dichloride at saturation coverage, a (1x1) LEED pattern should probably have been observed just as in the case for surface dihydride [29]. Our LEED studies indicate the presence of a (1x2) and (2x1) pattern for the whole range of Cl coverage. In addition, the Cl(a) coverage at the break point of the three coverage-dependent curves (fig.1, fig.3 and fig.4) gives a surface Cl to Si atom ratio of close to 0.7 (corresponds to SiCl(a)), instead of 2.0 (corresponds to $SiCl_2$(a)), which is consistent with the presence of the surface silicon monochloride species; (4) The observed single Si-Cl stretching mode at 553~600 cm^{-1} from HREELS agrees with that expected for the silicon monochloride species; (5) The core-level soft x-ray

photoelectron spectroscopy studies of Cl_2 adsorption on Si(100)-(2x1) have detected only monochloride species on the surface [30]. Thus, the surface monochloride is the major surface species produced by Cl_2 adsorption on Si(100)-(2x1) at 100K.

Apart from the major monochloride surface species, a small energy loss peak is observed at ~295 cm^{-1} (fig. 12 a-d). We assign this mode to the chlorine-to-silicon stretching mode for a bridge bonded chlorine species based on the following arguments: (1) Chlorine is known to form bridge bonded species in multicenter molecules. The structures of such bridge bonded Cl to Rh, Ir and Ru in metal complexes have been well documented [31]; (2) Molecules with bridge bonded chlorine to two Si atoms have been synthesized and the structure of these molecules has been determined [32]; (3) It has been observed that the bridge bonded Cl in the $(C_2H_5)_4Ga_2Cl_2$ molecule has a stretching frequency of 290~298 cm^{-1} [33] which is very close to the observed 295 cm^{-1} mode for Cl/Si(100); (4) Generally, bridge bonded Cl exhibits a lower stretching frequency than the terminally bonded Cl, such as in the Al_2Cl_6 molecule, where the terminally bonded Cl has a stretching frequency of ~625 cm^{-1} while the bridge bonded Cl has a stretching frequency of ~284 cm^{-1} [33]; in our Cl/Si(100) system, the terminally bonded Cl is at ~600 cm^{-1}, and the bridge bonded Cl is at ~295 cm^{-1}; (5) The alternative assignment of the 295 cm^{-1} vibration to the Si-Cl bending mode of surface monochloride seems inappropriate since not only is the frequency higher (by about 50~100 cm^{-1}) than what is expected for the bending mode, but also the relative intensity trend for the 295 cm^{-1} mode is opposite to the Si-Cl stretching mode at 600 cm^{-1} when the annealing temperature is changed; (6) The assignment of bridge-bonded Cl is supported by considerations of F/Si(100) system. Wu and Carter [34] have carried out a theoretical study of fluorine adsorption on Si(100)-(2x1). Their calculation indicates that F can also form a stable two-fold bridge bond to the substrate Si-Si dimer with a bond strength of 3.0 eV. Additionally, they predict that no barrier is associated

with the F diffusion from two-fold bridge bonding to one-fold terminal bonding. Bridge-bonded chlorine adsorbed on Si(100)-(2x1) has been theoretically investigated by Craig and Smith [35] using the SLAB-MINDO method. Their calculation predicts that the two-fold bridge bond adsorption structure is even more stable (by 0.61 eV per surface atom) than the monocoordinated adsorption structure; (7) Low temperature Cl_2 adsorption always gives a central Cl^+ beam in ESDIAD with four shoulder beams aligned along the [011] and [01$\bar{1}$] directions. These four shoulder beams intensify and are clearly resolved after annealing. This indicates that more than one kind of Cl bonding structure is present for low temperature Cl_2 adsorption [23]. The origin of the central Cl^+ beam in ESDIAD is attributed to the surface bridge bonded Cl (see more discussion in section 4.4); such symmetrical bridge bonded species have been predicted to give an ion emission beam directed along the surface normal [36] which corresponds to the observed central Cl^+ ESDIAD beam. These two structures for Cl adsorption on Si(100)-(2x1) are shown in fig. 14.

We suggest that the weak HREELS intensity for the bridge bonded Cl is mainly due to its small surface concentration, possibly coupled with a small dynamic dipole moment compared to terminal Si-Cl. The relatively high normal Cl^+ ion emission intensity from the small amount of bridge bonded Cl species is caused by the high ESD ionic cross-section of the bridge bonded Cl relative to that of the terminally bonded Cl. A high total (ionic and neutral) cross section for bridged-Cl relative to terminal-Cl has been demonstrated in the high current electron stimulated desorption experiments. The preferential electron stimulated desorption of the bridge bonded Cl has been observed (fig. 11a-b), which leads to an ESDIAD pattern transformation from a pattern dominated by a central Cl^+ beam to one dominated by four off-normal Cl^+ beams. The observed high relative ionic cross section (for Cl^+ production) and high relative total cross section (for Cl^+ and Cl production) for bridge bonded Cl suggests that

quenching of electronically excited bridged Cl species is less rapid than for terminal Cl species. Thus, ESDIAD, which measures Cl^+ ion emission, is highly sensitive to bridged Cl compared to terminal-Cl species.

4.3 Surface Disorder During Cl_2 Adsorption

The LEED results indicate a monotonic decrease of the intensity ratio for the half-order diffraction beam versus the first-order diffraction beam as a function of Cl_2 exposure. This is expected for random Cl_2 adsorption to produce Si-Cl species on the Si(100)-(2x1) substrate. In addition, the random distribution of the bridge bonded species could also be responsible for this effect.

4.4 Correlation of the ESDIAD Pattern With Surface Species Structure

From the HREELS measurements, low temperature Cl_2 adsorption results in both bridge bonded Cl(a) ($\nu(Si_2Cl)$~295 cm^{-1}) and terminally bonded Cl(a) ($\nu(SiCl)$~550-600 cm^{-1}). The former species is expected to produce a normal emission Cl^+ beam while the latter is expected to produce two off-normal Cl^+ emission beams as a result of the tilted Si-Cl bond. A Si(100)-(2x1) surface has orthogonal (1x2) and (2x1) domains as observed in LEED and STM studies [6,37]. The ESDIAD measurements sample both type of domains (electron beam spot size of ~1 mm diameter). Thus, four off-normal Cl^+ ion beams are expected for terminally bonded Cl(a) on symmetric Si_2 dimer sites. If the average areas of the (2x1) and (1x2) domains on the Si substrate are the same, a four fold symmetric Cl^+ ESDIAD pattern is expected from equal contributions of the two fold patterns. The superposition of the normal Cl^+ ion emission on the four beam pattern results in the observed centered ESDIAD pattern with the four shoulders along the [011] and [01$\bar{1}$] direction at low adsorption temperature. Upon annealing the substrate to 673K, the HREELS results indicate that the loss peak at ~295 cm^{-1}, corresponding to the $\nu(Si_2Cl)$ mode of the

bridge bonded Cl, has nearly disappeared. The ESDIAD pattern then changes to the four beam Cl^+ pattern.

4.5 The Irreversible Conversion of the Cl Bonding Configuration

The transformation of the broad centered Cl^+ ESDIAD pattern to the four beam Cl^+ pattern is observed to begin at about 273K and the transformation is completed at about 673K (fig. 7 b-e). This transformation has been observed for all initial chlorine coverages (figs. 5 and 6). In this temperature range (273-673K), little or no desorption of silicon chloride species is detected as indicated by TPD results (fig. 2), and no higher chlorides are observed from HREELS (fig. 12 and 13). Thus, we believe that the transformation of the centered Cl^+ ESDIAD pattern (120K) to a four beam pattern (673K) corresponds to the conversion of minority bridge bonded chlorine to terminally bonded chlorine rather than to other processes, such as desorption of certain surface species or formation of higher chlorides.

In addition, the complete transformation process extends through a large temperature range (273K ~ 673K). This transformation behavior suggests that the activation barrier and/or the pre-exponential factor increases/decreases as the extent of the conversion increases. A simple kinetic expression with constant activation energy and pre-exponential factor is incapable of describing a transformation process occurring over such a wide temperature range.

Since the chlorine structural conversion at elevated temperatures is from bridge bonding to terminal bonding, it is concluded that the terminally bonded Cl is thermodynamically more stable. This finding is opposite to the results obtained in a recent theoretical calculation [35]. Furthermore, the Cl bonding configuration change is an irreversible process since after annealing the Cl/Si(100) system to 673K, the cooling process does not restore the population of bridge bonded Cl producing the

normal Cl^+ ion emission beam (All ESDIAD data are collected at 120K.).

When dosing Cl_2 on a Si(100)-(2x1) substrate kept at 473K and 673K, similar ESDIAD patterns are observed just as for dosing Cl_2 at low temperature followed by annealing the crystal to the temperatures mentioned above. This further confirms that terminally bonded Cl is a thermodynamically more stable species, and the conversion from bridge bonded Cl to terminally bonded Cl is irreversible.

4.6 The Adsorption Sites for Cl(a) Giving Off-Normal Cl^+ in ESDIAD

The four beam ESDIAD pattern corresponds to terminal Cl adsorption on the symmetric dimer sites. If the surface species is composed of Cl bonded to both the symmetric dimer sites as well as to asymmetric sites, the different Si-Cl bond directions would give either split ESDIAD beams (possibly eight off-normal beams instead of four off-normal beams) or an unresolved off-center four beam pattern with an elliptical cross sectional contour for each beam. The fact that we only observe four off-center Cl^+ sharp beams, each with circular contour, suggests strongly that the Cl atoms are adsorbed on the dangling bonds of the symmetric dimer sites following annealing to ~673K.

Thornton et al. [7-8], in a recent study of chlorine adsorption using polarization dependent surface NEXAFS, conclude that the chlorine adsorption on Si(100)-(2x1) at ~500K leads to atop bonded chlorine on asymmetric Si-Si dimers with the Si-Cl bond oriented along the surface normal (accurate within 10°). Our ESDIAD results [fig. 7d] indicate that following annealing to about 500K, the majority of the Cl atoms are not bonded in this configuration. Instead, they are bonded to the Si with Si-Cl bond tilted off-normal (with an angle of ~25°±4° see section 4.8). In their NEXAFS measurement, a pseudo-intramolecular σ^*-resonance model was assumed valid and was employed to determine the Si-Cl bond orientation. ESDIAD is based on a real space

measurement and is believed to be more reliable and accurate for bond angle determination compared to NEXAFS [16a]. Moreover, a difference in the source of chlorine used in the two measurements may be a cause for the reported different Cl bonding configuration. We have used Cl_2 gas for adsorption. The NEXAFS study employed an electrochemical chlorine source. The possible production of atomic Cl as well as AgCl(g) from such a source may lead to different results [38].

A new ESDIAD report [39] has just come to our attention as we have nearly finished the writing of this manuscript. This work reports a three off-normal beam ESDIAD pattern for chlorine adsorption on Si(100)-(2x1) at room temperature and a single normal beam pattern after annealing to ~670K. They interpret their results as being indicative of the presence of the dichloride surface species following adsorption at room temperature with a thermally induced conversion to monochloride bonded at asymmetric Si-Si dimer sites at ~670K. These experimental results and the interpretation are inconsistent with our results reported here. The dichloride species are proposed [39] as a possible surface species without spectroscopic evidence for their presence. As we have discussed in section 4.1, our HREELS, our digital LEED study, and the cited photoemission study [30] exclude the dichloride surface species. Furthermore, our temperature dependent TPD and ESDIAD studies [section 3.2-3.3] indicate the importance of accurate surface temperature measurement for annealing a Cl-covered Si(100) surface. If the temperature exceeds 750K, the substrate etching process will occur (fig. 2). This causes the production of a random array of Si-Cl bond orientations which when averaged will give the appearance of an average normal Si-Cl bond orientation as shown in fig. 7f. We have employed a calibrated thermocouple and feedback control of an electronic temperature programmer for accurate temperature control [40], while an optical pyrometer was used for temperature measurement in ref. 39.

4.7 Si-Cl Bond Polar Angle

Detailed measurements of the four beam ESDIAD patterns of the terminally bonded monochloride species allow us to estimate the Si-Cl bond tilt angle. Due to the limited detection solid angle of the ESDIAD apparatus, a positive bias was applied to the crystal which compresses the Cl^+ ion trajectories to a smaller polar angle. A series of different bias voltage measurements were carried out showing that the ion emission angle, θ_m, increases as the bias voltage is decreased (fig. 15). The behavior of the Ci^+ ion emission angle, θ_m, fits well within the calculated shaded region in an energy range between E_0 = 0.8 eV and E_0 = 1.7 eV as obtained from an ion optics computer simulation. The field-free ion emission angle, θ_0, ranges from 25°- 31° (at zero bias) over the 0.8-1.7 eV energy range according to the model. The best fit for our data involves a Cl^+ initial ion kinetic energy, E_0=1.1 eV, and a zero bias ion emission angle θ_0 = 27°. This calculation is more thoroughly described in the appendix.

The final state effects of image potential and reneutralization can influence the zero field ion desorption angle, θ_0, by distorting the ion trajectories and the angular distributions. Several theoretical papers have addressed the influence of the image force [41-46] and the reneutralization effect [42, 47-49] on ion angular distribution measurements. The attractive image potential increases the measured polar angle of the ion escaping from the surface while the reneutralization acts in an opposite sense to the image field to decrease the measured polar angle. These two effects tend to cancel each other, especially for small polar desorption angles [46-47]. Madey et al. have carried out theoretical studies in which both image charge and reneutralization effects are taken into account in order to obtain the true chemical bond angle (θ_{bond}) from the laboratory measured ion emission angle (θ_0 at zero bias voltage) [47]. Using their methods, the Si-Cl bond polar angle, after the correction for the image potential and

reneutralization effects, is 25°±4° (see appendix).

4.8 Si-Cl Bond Azimuthal Orientation

The two Si-Cl bonds formed on the Si-Si dimer sites can be either co-planar to the Si-Si dimer bond or they can be twisted from the vertical Si-Si dimer bond plane if the repulsive interaction between Cl adsorbed on neighbor Si-Si dimer sites becomes significant. After comparing the orientation of the four beam ESDIAD pattern (two fold symmetry for both domains) with that of the two domain LEED pattern, we conclude that there is no observable ($< 1°$) amount of twisting of the Si-Cl bonds with respect to the Si-Si dimer bond. Theoretically, Wu and Carter [34] have shown that the repulsive interaction between surface monofluoride species is not enough to produce considerable Si-F bond twisting from the vertical plane containing Si-Si dimer bond. This is consistent with our monochloride results. Wu and Carter [34] predict that a repulsive interaction may become large for neighboring surface difluoride species leading to a large amount of bond twisting.

4.9 The Adsorption Sites for Cl(a) Giving Normal Cl^+ in ESDIAD

Our ESDIAD and HREELS results are consistent with the interpretation that the Cl species adsorbed on bridge sites produces a normal Cl^+ emission beam. Other adsorption sites have been considered as well for rationalizing the Cl^+ emission along the surface normal direction. The first model considered is Cl adsorption on asymmetric Si-Si dimer sites. Regardless of the controversy reported in the literature for [50] or against [51] the use of the asymmetric dimer model on clean Si(100)-(2x1), the following reasoning argues against using this model to explain the Cl adsorption experiments in this paper: (1) In an asymmetric dimer, one dangling bond is expected to tilt toward the surface normal while the other dangling bond would tilt away from the surface normal [13-14, 50]. For an assumed Si-sp^3 hybridized orbital, it is

expected that the symmetric Si-Si dimer would project the dangling bond away from the surface normal by about 20°. Studies have shown that the Si-Si dimer bond for the asymmetric configuration only tilts about 12° with respect to that of the symmetric configuration for the clean Si (100) surface [52]. If the ~110° angle between the dangling bond and the dimer bond of the same Si atom remains for the asymmetric dimer, then one of the dangling bonds for the asymmetric configuration would therefore have tilted about 12° toward the surface normal from the previous symmetric configuration involving a 20° tilt angle, resulting in a dangling bond which projects in a direction 8° from the surface normal. The two domain Si(100) surface would therefore produce four Cl^+ beams tilted 8° away from the surface normal. These 8° tilted beams were not detected in our ESDIAD studies of the normal Cl^+ beam at various crystal bias potentials; (2) The transformation of the centered Cl^+ beam to four 25° off-normal beams observed in ESDIAD requires a high activation energy to surmount the conversion barrier since the site conversion occurs for Cl/Si over a wide range of higher temperatures (273K–673K). It is difficult to imagine a physical model to account for the origin of this high barrier since the asymmetric-symmetric conversion process for clean Si_2 dimer sites is reported to occur with an activation energy corresponding to a rapid process at ~300K [52]. (3) Schnell et al. [14] have studied Cl_2 dissociativeiy adsorbed on Ge (001)-(2x1) with photoemission. They have argued that after Cl_2 adsorption, the substrate should contain symmetric dimers since the electrons of the dangling bonds can now bond to Cl and have no tendency to pair up causing asymmetric dimer formation.

The second model considered to account for the Cl^+ emission beam along the surface normal direction is Cl adsorption on defect sites. Recently, it was shown that O_2 adsorption on Si(100)-(2x1) at room temperature results in Si atom ejection. STM measurements indicate the number of surface asperities increase with the O_2 exposure,

and they tend to appear near reaction-induced dark sites as seen in the STM [53]. If the same effects were present for Cl_2 adsorption at low temperature (~100K), the random orientation of the Si-Cl bonds on defect sites could produce a centered ESDIAD beam representing an average of Si-Cl bond directions on defects. However, defect sites such as Si adatoms or vacancies would have more unsaturated coordination sites, and would be expected to lead to formation of higher surface chlorides. Our HREELS results do not indicate the presence of the higher (than mono-) chloride surface species after low temperature chlorine adsorption (fig. 12). The results from core-level soft x-ray photoelectron spectroscopy [30] also support our HREELS observation of monochloride surface species. In addition, the low temperature ESDIAD pattern with a prominent normal Cl^+ beam and the four shoulders is similar for all coverages of Cl(a), suggesting that preferential adsorption on defects is not involved. Thus, the defect sites model is unlikely to account for the centered Cl^+ ESDIAD beam following Cl_2 adsorption at low temperature.

4.10 The Cl^+ Ion Yield

The Cl^+ ion yield exhibits an interesting trend as a function of Cl_2 exposure. A distinct maximum is observed at an intermediate Cl_2 exposure (1.2×10^{14} molecules/cm^2) (fig . 9). A similar coverage effect has been reported for the O^+ yield in ESD from CO/Ni(111) [54]. This effect is postulated to be due to provision of additional channels for quenching of electronically excited species at higher adsorbate coverages [54]. An increase of Cl surface concentration would lead to a proportional increase of the ESD ion yield assuming a constant ESD cross section. This accounts for the initial monotonic increase in the Cl^+ ion yield with increasing Cl_2 exposure (fig. 9). At higher coverage, we postulate that adsorbate-adsorbate interactions lead to enhanced quenching of excited Cl(a) species and to the eventual decrease in Cl^+ yield at Cl(a) coverages above approximately one-half monolayer.

At the maximum yield, about 4×10^{-7} Cl^+/e are desorbed from approximately one-half monolayer of Cl(a) at $V_e = 120$ V.

4.11 Retarding Field Measurements of the Cl^+ Ion Energy Distribution

The ESDIAD apparatus was employed as a retarding field analyzer for study of the Cl^+ energy distribution as shown in fig. 10. Measurements of this type are unreliable (~1 eV error) because of unknown contact potentials between the substrate and the retarding grid. Thus, the most probable Cl^+ energy (~0.3 eV) is likely to be inaccurate by as much as 1 eV, although the FWHM (0.6 eV) of the Cl^+ ion energy distribution will be accurate.

We consider the use of the ion optical transmission characteristics of the ESDIAD apparatus to be a more reliable method for estimating the most probable Cl^+ kinetic energy. The value obtained for the most probable Cl^+ kinetic energy using this method is $1.1^{+}_{-}{}^{0.6}_{0.3}$ eV, as shown in fig. 15, and as discussed in the appendix.

4.12 The Etching of the Si(100) Surface by Chlorine

Temperature programmed desorption spectra (fig.2) indicate that an etching process is initiated at ~800K for submonolayer Cl(a) coverage, producing $SiCl_2(g)$. For high Cl(a) coverages, an additional etching channel occurs at ~500K producing $SiCl_4(g)$ (fig. 2). Since higher silicon chloride surface species are not observed by HREELS for Cl_2 adsorption at low temperature, chlorine has not penetrated at 100K into the second layer of the substrate, breaking Si-Si backbonds. When the silicon dichloride species is formed at elevated temperatures, the repulsive interaction between $SiCl_2(a)$ species and neighboring species, coupled with reduced Si bonding to substrate Si may lead to the immediate desorption of $SiCl_2$ into the gas phase. This is possibly the reason that we have not detected the surface dichloride species at all the

temperatures employed in the HREELS study. A similar repulsive interaction has been predicted for surface difluoride species [34].

5. Summary

The adsorption of Cl_2 on Si(100)-(2x1) has been studied at 100K, and the thermal behavior of the chlorine layer from 100K - ~ 1000K has been studied using a combination of experimental techniques. The basic findings of this work are summarized below:

(1) The adsorption rate of Cl_2 by Si(100)-(2x1) at 100K is initially high, and is directly proportional to Cl_2 fluence up to a coverage of ~0.7 Cl/Si. Above this coverage, much slower Cl_2 uptake kinetics are observed.

(2) Cl_2 adsorption at 120K results in a decrease in surface order as indicated by the reduction in the relative intensity of the one-half order LEED beams.

(3) At 120K, adsorption of Cl_2 produces two surface species, a majority species with inclined Si-Cl bonds associated with symmetric Si_2 dimer sites, and a minority bridged Si_2Cl species bonded to adjacent Si atoms on symmetric Si_2 dimer sites. The minority Si_2Cl species has a high cross section (ionic and total) for ESD compared to the inclined Si-Cl species and produces a normal Cl^+ ESDIAD beam.

(4) Both surface monochloride [ν(SiCl) of 550 – 600 cm^{-1}] and bridged Cl [$\nu(Si_2Cl)$ of ~ 295 cm^{-1}] are observed by HREELS. Cl_2 adsorption does not lead to production of observable coverages of $SiCl_2$(a) or of higher silicon chlorides.

(5) Conversion of bridged Si_2Cl species to inclined Si-Cl species occurs over a temperature range of 273K-673K, forming the more stable inclined Si-Cl species.

(6) The tilt angle for Si-Cl bonds on the symmetric Si_2 dimer sites is $25^\circ \pm 4^\circ$ off-normal, corrected for ion optics effects, the ion image potential effect, and the ion reneutralization effect.

(7) Strong interatomic Cl(a)-Cl(a) quenching effects in ESD have been observed. These lead to a reduction in Cl^+ ion yield above ~1/2 ML Cl coverage.

(8) The Cl^+ ion energy distribution has been measured and the most probable Cl^+ kinetic energy is estimated to be $1.1^{+\ 0.6}_{-\ 0.3}$ eV using the ion transmission behavior of the ESDIAD analyzer. Measurements with the ESDIAD optics used as a retarding field analyzer give results in satisfactory agreement with this.

(9) Heating of the high coverage Cl(a) layer yields $SiCl_2(g)$ species near 800K, causing silicon etching. At higher Cl(a) coverages, $SiCl_4(g)$ is also evolved near 500K.

Appendix: Ion Optics Computer Simulation and Estimation of the Image Potential and Reneutralization Effects

Detailed measurements of the four beam Cl^+ ESDIAD patterns from the terminally bonded monochloride species allow us to evaluate the Si-Cl bond tilt angle. This consists of two steps: (1) to obtain a Cl^+ ion emission angle under a field free condition, and (2) to correct this ion emission angle for the final state effects so that the Si-Cl chemical bond angle is obtained.

Direct measurement of the field-free Cl^+ ion emission angle is prohibited due to the limited solid angle detected by the current ESDIAD apparatus. Therefore, determination of the final Cl^+ ion emission angle under a field-free condition is done

by measuring the Cl^+ ion emission angles at various crystal bias voltages and then comparing the experimental data with the results obtained from computer simulation, in order to accurately extrapolate the angle to the field free case. The consequence of applying a positive bias on the crystal is a compression of the Cl^+ ion trajectories into smaller polar angles (θ_m), compared to that at a field-free condition (θ_0) (see inset of fig. 15). The behavior of the Cl^+ ion trajectories under different crystal bias voltages was investigated, and the data are shown by the filled circles in fig. 15. The error bars indicated are evaluated from the deviation of angles measured from both domains of Si dimers. However, for the data shown at the crystal bias voltages of 3.0 and 4.0 V, only one off-normal beam ejected from each dimer domain was observable, and thus, the error bars for these two data points are not given in this case. The presence of only one beam from each dimer domain at low bias voltages is due to the fact that the incident electron beam is intercepted by the crystal surface somewhat off the center axis of the ESDIAD apparatus.

The ion trajectories were simulated by a SIMION computer program from the Idaho National Engineering Laboratory, EG&G Idaho Inc. In the simulation, the accuracy of the physical dimensions of the ESDIAD ion optics is 1 mm; the mass/charge ratio (AMU per unit charge) of 35.5, averaging from the natural abundance of Cl isotopes, is used for the Cl^+ ion; and the lower limit for the maximum absolute voltage change occurring at any point during the simulation is 0.005 eV. The results of the computer simulation with different ion kinetic energies (E_0) and different emission angles (θ_0) are shown in figs. 15 and 16. Although the distribution of the scattered experimental data can certainly be confined in fig. 15 within the two extremes of E_0 = 1.7 eV, θ_0 = 31° and E_0 = 0.8 eV, θ_0 = 25°, the experimentally observed Cl^+ ion emission angle versus the crystal bias voltage is best fitted with E_0 = 1.1 eV, θ_0 = 27°. The difference of the kinetic energy between the best-fitted result

from simulation (1.1 eV) and the observed maximum Cl^+ ion energy distribution by the retarding potential method (~ 0.3 eV, see fig. 10) is believed to be mainly due to the unknown work function difference between the crystal and grids in the ESDIAD apparatus.

Examples of the ion trajectory calculations for the ESDIAD analyzer are shown in fig.16. Two physical results are presented illustrating the analyzer behavior and the sensitivity to the parameters used in the calculation. Fig.16a shows the effect of decreasing the crystal bias voltage from +10 V to +6 V on the measured ion emission angle (θ_m). Fig.16b shows the effect of changing the kinetic energy of a Cl^+ ion from 0.8 eV to 1.7 eV at a crystal bias voltage of +10 V and an initial emission angle of 27°. It may be seen that the transmission characteristics of the analyzer may be sensitively employed to determine the kinetic energy of an ion which will be transmitted within an allowed angular range.

For step two of this procedure involving consideration of image potential and ion neutralization effects, theoretical studies have been published [47] in which both ion image potential (V_I) and ion reneutralization effects are taken into account to obtain the chemical bond angle (θ_{bond}) from the laboratory-measured field free ion emission angle (θ_0). A simple classical picture was used in the previous theoretical study: a quasi-impulsive central force ejects an ion along the chemical bond direction; the surface is an ideal planar conductor; and the ion reneutralization rate depends only on the distance z above the surface. The following assumptions have been employed in ref. 47: (1) A Hagstrum non-local reneutralization process where the reneutralization rate R depends only on the ion-surface separation z: $R(z) = A\, e^{-az}$ where z_0 is the initial distance of the image charge from the image plane; (2) A Morse electronic ground state potential; (3) A Born-Mayer repulsive ion potential: $V(r) = B\, e^{-br}$; and (4) A harmonic ground state vibrational wave function. The ratio of the image

potential (V_I) at the starting point of the ion ejection to the ion initial kinetic energy (E_0) determines the extent of the ion trajectory deflection toward the surface by the image force, while the reneutralization process (determined by the pre-exponential factor, A, the exponential factor, a, and the resident time near the surface region, ($\sim v_0^{-1}$)), governs the distortion of the distribution of the detected ion trajectories from their initial assumed Gaussian distribution. The result of the reneutralization process is that trajectories further away from the surface have larger probabilities of being detected. The correction introduced by considering the combination of image potential and reneutralization effects gives a correlation of the experimentally observed ion emission angle (θ_0) with the chemical bond angle (θ_{bond}) as follows [47]:

$$\arcsin y = \theta_{bond} - \frac{\theta_w^2}{2} y \left[\frac{1-\beta}{(\beta - y^2)\sqrt{1-y^2}} + \frac{A}{av_0}\sqrt{1-y^2}\, K(y;\beta,\delta)\right] \qquad (1)$$

where $y = \sqrt{\beta}\, \sin\theta_0$

and $\beta = 1 - |V_I| / E_0$

$\delta = 1/(az_0)$

$$K(y;\beta,\delta) = \int_0^\infty (\beta - y^2 + \frac{1-\beta}{1+\delta\xi})^{-3/2} e^{-\xi}\, d\xi$$

θ_w is the half width obtained from the Gaussian approximation for the ESD excitation probability distribution [47]. A replot of the calculated result for the O/W(100) system is presented in fig. 17 for comparison with the Cl/Si(100) results. A new abscissa (the laboratory-measured ion emission angle θ_0) is employed instead of the chemical bond angle used in ref. 47. This plot is identical to that obtained from the treatment in ref. 47 showing that our analysis methodology is in agreement with the earlier work.

For the Cl^+ ions desorbed from the Si(100) surface, we used identical parameters to those in ref. 51 ($A/a = 8x10^4$ m/s and $a = 3$ Å^{-1}) for the reneutralization process based on the same Hagstrum non-local reneutralization assumption. The image potential V_I can be estimated as follows for semiconductors [49, 55]:

$$V_I = - \frac{(\varepsilon - 1)}{(\varepsilon + 1)} \frac{q^2}{4z_0} \qquad (2)$$

where q is the charge of the ion and z_0 is the initial distance of the image charge to the image plane. ε is the static dielectric constant for the medium. For a Si substrate, $\varepsilon = 11.9$ [56]. Since no data are available for the position of the image plane, we estimate the image potential assuming the image plane is the surface plane passing through the Si atom nuclei. This gives z_0 as the Si-Cl bond length ($d = 2.03 \pm 0.02$ Å [7-8, 57]) multiplied by the cosine of the laboratory observed bond angle (27°). With this assumed image plane position we can calculate the first order correction for the Si-Cl bond angle. Using the new bond angle and the new image potential, a second order correction is obtained. This calculation loop converges to a bond angle of 25°.

The ion initial kinetic energy is estimated as $E_0 = E_\infty + |V_I|$, where E_∞ is from our analysis shown in fig.15 (~ 1.1 eV). The initial ion velocity (v_0) is obtained from E_0. θ_w is derived from the experimental value of 11°. The maximum and minimum for the parameter $\delta = (a.z_0)^{-1}$ can be estimated to get an upper and lower limit for the correction. Since the exponential factor, $a \sim 3$ Å^{-1} , is a finite number determined by the nature of the reneutralization, we estimate the limit for δ based on z_0:

$$\delta_{max} = (a \cdot z_{0\,min})^{-1} = (a \cdot d \cdot \cos\theta_{max})^{-1}$$

$$\delta_{min} = (a \cdot z_{0\,max})^{-1} = \lim_{z_0 \to \infty} (a.z_0)^{-1} = 0$$

The θ_{max} can be estimated from the critical angle, $\theta_c = \cos^{-1}(|V_I|/E_0)^{1/2}$, and is the maximum ion emission angle above which the image force will bend the ion trajectory back to the surface [46-47]. The value of θ_c is 39° for Cl/Si(100) which gives $z_{0\,min} \sim 1.58$ Å.

Using these parameters, the angular correction, λ, for the image potential and reneutralization effects for Cl/Si(100) is shown in fig. 18. At a measured emission angle of 27°, the correction, λ, is 2°. This results in an Si-Cl polar angle of $25^\circ \pm 4^\circ$.

Acknowledgments

The authors would like to acknowledge the Office of Naval Research for their financial support of this work. We would like to thank Professor. H. J. Jänsch who assisted with improvements of ESDIAD apparatus, to Mr. S. R. Lucas for helping with initial thermal desorption experiments, to Professor G. Thornton et al. for preprints of their NEXAFS results, to Professor E. Carter et al. for preprints of the F/Si(100)-(2x1) calculation, to Professor R. Allen et al. for preprints of a molecular dynamical simulation, to Professor J. Yarmoff et al. for their XPS results for Cl/Si(100), to Dr. David A. Dahl for providing the SIMION program used in the ion optics simulation, and to Professor E. M. Williams et al. for a preprint concerning their Cl_2 adsorption study on Si(100)-(2x1).

References

1 J. W. Coburn and H. F. Winters, J. Appl. Phys. 50 3189 (1979).

2 N. Aoto Takasaki, E. Ikawa and Y. Kurogi, J. Vacuum Sci. Technol. B4 806 (1986).

3 E. Ikawa, S. Sugito, N. Aoto and Y. Kurogiin :Proc. Symp. on VLSI Technology, May 18-21, Karuizawa, Japan p.27 (1987).

4 E. Sirtl, L. P. Hunt and D. H. Sawyer, J. Electrochem. Soc. 121 919 (1974).

5 W. A. P. Claassen and J. Bloem, J. Crystal Growth 50 807 (1980).

6 J. E. Rowe, G. Margaritondo and S. B. Christman, Phys. Rev.B 16 1581 (1977) .

7 D. Purdie, C. A. Muryn, N. S. Prakash, K. G. Purcell, P. L. Wincott, G. Thornton and D. S.-L. Law, Proc. of XAFS VI., in press.

8 (a) D. Purdie, C. A. Muryn, N. S. Prakash, K. G. Purcell, P. L. Wincott, G. Thornton and D. S.-L. Law, Phys. Rev. Lett. (submitted); (b) J. Phys.:Condens Matter 3 7751 (1991).

9 G. Thornton, P. L. Wincott, R. M. Grath, I. T. McGovern, F. M. Quinn, D. Norman and D. D. Vvedensky, Surf. Sci. 211/212 959 (1989).

10 L. S. O. Johnasson, R. I. G. Uhrgerg, R. Lindsay, P. L. Wincott and G. Thornton, Phys. Rev. B42 9534 (1990).

11 R. B. Jackman, H. Ebert and J. S. Foord, Surf. Sci. 176 183 (1986).

12 (a) N. Aoto, E. Ikawa and Y. Kurogi, Surf. Sci. 199 408 (1988). (b) ibid, 250 235(1991).

13 R. M. Tromp, R. J. Hamers and J. E. Demuth, Phys. Rev. Lett. 551 303 (1985).

14 R. D. Schnell, F. J. Himpsel, A Dogen, D. Rieger and W. Steinmann, Phys. Rev. B32 8052 (1985).

15 J. J. Czyzewski, T. E. Madey, J. T. Yates, Jr., Phys. Rev. Lett., 32 777 (1974).

16 (a) R. D. Ramsier and J. T. Yates, Jr., Surf. Sci. Rep. 12 (6-8) 243 (1991). (b) T. E. Madey, Science 234 316 (1986). (c) J. T. Yates, Jr., M. D. Alvey, M. J. Dresser, M. A. Henderson, M. K. Kiskinova, R. D. Ramsier and A. Szabo,Science 255 1397 (1992).

[17] (a) R. M. Wallace, P. A. Taylor, W. J. Choyke and J. T. Yates, Jr., Surf. Sci., 239 1;1990 (b) R. M. Wallace, C. C. Cheng, P. A. Taylor, W. J. Choyke and J. T. Yates, Jr.,Appl. Surf. Sci. 45 201;1990 (c) R. M. Wallace, P. A. Taylor, W. J. Choyke and J. T. Yates, Jr., J. Appl. Phys. 68 3669 (1990).

[18] (a) M. J. Dresser, M. D. Alvey and J. T. Yates, Jr., Surf. Sci. 169 91; 1986 (b) R. W. Wallace, P. A. Taylor, M. J. Dresser, W. J. Choyke and J. T. Yates, Jr., Rev. Sci. Instrum. 62 720 (1991).

[19] A. Szabó, M. Kiskinova and J. T. Yates, Jr., Surf. Sci., 205 207 (1988).

[20] M. J. Bozack, L. Muehloff, J. N. Russell, Jr., W. J. Choyke and J. T. Yates, Jr., J. Vac. Sci. & Technol. A5 1 (1987).

[21] (a) C. T. Campbell, S. M. Valone, J. Vac. Sci. & Technol. A3 408; 1985 (b) A. Winkler and J. T. Yates, Jr., J. Vac. Sci. & Technol. A6 2929 1988;(c) C. C. Cheng, R. M. Wallace, P. A. Taylor, W. J. Choyke and J. T. Yates, Jr., J. Appl. Phys. 67 613 (1990).

[22] J. E. Crowell, J. G. Chen and J. T. Yates, Jr., Surf. Sci. 165 37 (1986).

[23] C. C. Cheng, Q. Gao, W. J. Choyke and J. T. Yates, Jr., submitted to Phys. Rev. B.

[24] (a) K. Nakamoto, in "Infrared Spectra of Inorganic and Coordination Compounds", 4th ed., John Wiley & Sons, Inc., New York, , p.132; 1986 (b) M. C. Tobin, J. Am. Chem. Soc., 75 1788 1953; (c) K. Shimizu and H. Murata, Bull. Chem. Soc., Japan, 32 46 1959; (d) L. Burnelle and J. Duchesne, J. Chem. Phys. 20 1324 1952; (e) J. Lanne, Spectrochimica Acta 26A 517 (1970).

[25] (a) H. Ibach, H. Wagner and D. Bruchman, Solid State Commun. 42 457(1982);(b) F. Stucki, J. Anderson and G. J. Lapeyre and H. H. Farrell, Surf. Sci. 143 84 (1984); (c) J. A. Schaefer, F. Stucki, D. J. Frankel, W. Gopel and G. J. Papeyre, J. Vacuum Sci. Technol. 82 359 (1984).

[26] K. Nakamoto, in "Infrared Spectra of Inorganic and Coordination Compounds", 4th ed., John Wiley & Sons, Inc., New York, p. 101 (1986).

[27] H. Ibach and D. L. Mills, "Electron Energy Loss Spectroscopy and Surface Vibrations", Academic Press, New York, (1982).

[28] unpublished results of $SiCl_4$ adsorption on Si(100)-(2x1) studied with HREELS.

[29] C. C. Cheng and J. T. Yates, Jr., Phys. Rev. B43 (5) (1990) 4041, and references therein.

[30] J. A. Yarmoff et al., private communication.

[31] Comprehensive Organometallic Chemistry, Vol.5, p. 298, p. 300 and reference therein, Vol. 4, p. 901 and references therein, eds. G. Wilkinson, F. Gordon, A. Stone and E. W. Abel, Pergamon Press, New York, (1982).

[32] (a) M. Weidenbruck, K. Kramer, A. Schafer and J. K Blum, Chem. Ber. 118(1985)107; (b) M. Weidenbruch, K. Kramer, Z. Naturforsch.,B:Anorg. Chem.,Org. Chem., 40B, 601 (1985) .

[33] E. Maslowsky, " Vibrational Spectra for Organometallic Compounds", John Wiley & Sons, Inc., New York, , p. 61 (1977).

[34] C. J. Wu and E. A. Carter, Phys. Rev. B, to be published.

[35] B. I. Craig and P. V. Smith, Surf. Sci. 282 235 (1992).

[36] E. Preuss, Surf. Sci. 94 249 (1980).

[37] J. J. Boland, Surf. Sci. 261 17 (1992).

[38] (a) N. D. Spencer and R. M. Lambert, Surf. Sci. 107 237 (1981). (b). N.D. Spencer, P. J. Godard, P. W. Davies, M. Kitson and P. M. Lambert, J. Vac. Sci. Technol., A1 1554 (1983). (c) M. Kitson and R. M. Lambert, Surf. Sci. 100 368 (1980).

[39] S. L. Bennett, C. L. Greenwood and E. M. Williams, DIET V, New Mexico, 1992, in press.

[40] R. J. Muha, S. M. Gates, P. Basu, and J. T. Yates, Jr. Rev. Sci. Inst., 56 613 (1985).

[41] (a) T. E. Madey and J. T. Yates, Jr., Surf. Sci. 63 203 (1977). (b)T. E. Madey, in:"Inelastic Particle-Surface Collisions", Springer Series in Chemical Physics, Vol. 17, eds. W. Heiland and E. Taglauer, Springer, Heidelberg, p. 80 (1981).

[42] P. J. Feibelman, in: "Desoprtion Induced by Electronic Transitions, Springer Series in Chemical Physics", Vol. 24, eds. N. H. Tolk, M. M. Traum, J. C. Tully and T. E. Madey, Springer, Heidelberg, p. 61 (1983).

[43] D. E. Ramaker, J. Vacuum Sci. Technol. A1 1137 (1983).

[44] W. L Clinton, Surf. Sci. 112 L791 (1981).

[45] R. A. Gibbs, S. P. Holland, K. E. Foley, B. J. Garrison and N. Winograd, Phys. Rev. B24 6178 (1981).

[46] Z. Mišković, J. Vukanic' and T. E. Madey, Surf. Sci. 141 285 (1984).

[47] Z. Miškovic', J. Vukanic' and T. E. Madey, Surf. Sci. 169 405 (1986).

[48] D. P. Woodruff, Surf. Sci. 124 320 (1983).

[49] W. L. Clinton, M. Esrick, H. Ruf and W. Sacks, Phys. Rev. B31 722 (1985).

[50] G. K. Wertheim, D. M. Riffe, J. E. Rowe and P. H. Citrin, Phys. Rev. Lett., 67 120 (1991) and references therein.

[51] D. S. Lin, T. Miller and T.-C. Chiang, Phys. Rev. Lett. 67 2187, (1991) and references therein.

[52] (a) J. Cryko and R. E. Allen, 38th National Symp. Am. Vac. Soc., Seattle, p. 317, (1991) and manuscript to be submitted. (b) R. A. Wolkow, Phys. Rev. Lett. 68 2636 (1992).

[53] D. G. Cahill and Ph. Avouris, Appl. Phys. Lett. 63 (3) 326 (1992).

[54] (a) F. P. Netzer and T. E. Madey, J. Chem. Phys. 76(1) 710 (1982). (b) T. E. Madey, J. T. Yates, Jr., A. M. Bradshaw and F. M. Hoffman, Surf. Sci., 89 370 (1979).

[55] H. Sun and S. W. Gu, Phys. Rev. B 41 3145 (1990).

[56] $\varepsilon = 11.9$ for Si(100) in "Data in Science and Technology, Semiconductors, Group IV elements and III&V Compounds", eds. O. Madelung, R. Poerschke, Springer-Verlag, New York, p. 20 (1991).

[57] The Si-Cl bond length averaged from $SiCl_4$, Si_2Cl_6, SiH_3Cl, SiH_2Cl_2 compounds is 2.03±0.02 Å. "Handbook of Chemistry and Physics", 63 Ed., CRC Press Inc., Boca Raton, FL, p. F181-183 (1982-83).

Figure Captions

Fig. 1. Kinetics of Cl adsorption from Cl_2 on Si(100)-(2x1) at 100K. E_{beam} = 2kV.

Fig. 2. Temperature programmed desorption following Cl_2 adsorption on Si(100)-(2x1) at 120K. The heating rate is ~3.6K/sec. The Cl_2 exposures are (a) $0.5x10^{14}$ molecules/cm^2; (b) $1.0x10^{14}$ molecules/cm^2; (c) $2.6x10^{14}$ molecules/cm^2; and (d) $4.6x10^{14}$ molecules/cm^2.

Fig. 3. The TPD yield of $SiCl_2$ and $SiCl_4$ after Cl_2 adsorption on Si(100)-(2x1) at 120K.

Fig.4. The LEED intensity ratios (averaged for both (2x1) and (1x2) domains) for half-order diffraction beams versus first order diffraction beam as a function of Cl_2 exposure at 120K.

Fig. 5. ESDIAD patterns following Cl_2 adsorption on Si(100)-(2x1) at 120K. The crystal is biased at +10V. Cl_2 exposures are (a) $0.5x10^{14}$ molecules/cm^2; (b) $1.3x10^{14}$ molecules; and (c) $2.6x10^{14}$ molecules/cm^2. The relative amplification factors are indicated. Each 3-dimensional plot is accompanied by a contour plot obtained at increments of 1/6 of the peak maximum.

Fig. 6. ESDIAD patterns following annealing of the Cl/Si(100)-(2x1) surfaces to 673K for 60 seconds. (Data were collected at 120K). The Cl_2 exposures correspond to those in fig. 5. The relative amplification factors are indicated. Contour profiles are obtained at increments of 1/6 of the peak maximum.

Fig. 7. Temperature dependent ESDIAD of Cl_2/Si(100)-(2x1). Cl_2 adsorption at 120K (exposure of $2.4x10^{14}$ molecules/cm^2) followed by annealing the crystal to the following temperatures for 60 sec.(a) 120K; (b) 273K; (c) 423K; (d) 523K; (e) 673K and (f) 823K. The relative amplification factors are indicated. Contour profiles are obtained at increments of 1/6 of the peak maximum. All measurements are made at 120K.

Fig 8. Cross section view of the temperature dependent ESDIAD patterns for Cl_2/Si(100)-(2x1). The experimental conditions for (a) - (f) correspond to those in fig. 7 (a) - (f).

Fig. 9. Cl^+ ion yield measured using ESDIAD apparatus as a function of Cl_2 exposure. V_e=120 V and I_e=6 nA. Results for both the low temperature adsorption (circles) and after annealing to 673K for 60 seconds (squares) are shown.

Fig. 10. Kinetic energy distribution of Cl^+ ion measured using the retarding potential method in the ESDIAD apparatus. Cl_2 was adsorbed on Si(100)-(2x1) at 120K and then annealed to 673K for 60 sec. Cl_2 exposure = $1.2x10^{14}$ molecules/cm^2.

Fig. 11. Effect of high electron bombardment flux on Cl(a) species. Cross-section view of ESDIAD pattern: (a) 120K Cl_2 adsorption on Si(100)-(2x1) (exposure=$2x10^{14}$ molecules/cm^2), and (b) After exposing the previous surface to $4.5x10^{18}$ electrons/cm^2 at 120K. The intensities in the plot are normalized to the same number of Cl^+ ion counts in the ESDIAD pattern. Crystal bias = + 10 V. E_e = 170 eV.

Fig. 12. Coverage dependent HREELS for Cl_2 adsorption on Si(100)-(2x1) at 100K. Cl_2 exposures are (a) $0.5x10^{14}$ molecules/cm^2; (b) $2.2x10^{14}$ molecules/cm^2; (c) $3.2x10^{14}$ molecules/cm^2; and (d) $7.4x10^{14}$ molecules/cm^2.

Fig. 13. Temperature dependent HREELS for Cl_2 adsorption on Si(100)-(2x1). Cl_2 exposure is $7.4x10^{14}$ molecules/cm^2 (a) adsorption at 100K; (b) after 473K annealing; (c) after 673K annealing and (d) after 875K annealing. All spectra are collected at 100K.

Fig. 14. Proposed Cl bonding configurations on Si(100)-(2x1).

Fig. 15. Cl^+ measured emission angle, θ_m, for the four beam ESDIAD pattern versus V_{bias} on crystal. The initial Cl_2 exposure is $2.6x10^{14}$ molecules/cm^2. The error from the experiment is evaluated from the average of angles measured from the two domains. The solid lines are computer simulations for the ion emission angles as a function of crystal bias voltage.

Fig. 16. Examples of Cl^+ ion trajectory calculations in the ESDIAD analyzer. (a) effect of changing the positive crystal bias, V_{bias}; (b) effect of changing the Cl^+ ion energy from 0.8 eV to 1.7 eV; V_{bias} = +10 V, θ_0=27°.

Fig. 17. Corrections for the image potential and reneutralization effects on the measured ion emission angle (after Z. Mišković et al. [47], with a different x-axis, for O^+ from W(100)). This figure is given to tie together the analysis in this paper and ref. 47.

Fig. 18. Corrections for the image potential and reneutralization effects on the measured ion emission angle (Cl^+ from Si(100)).

Table 1. Vibrational Frequencies for Silicon Chlorides (cm^{-1})

	υ_a	υ_s	δ	γ
$SiCl_4$ (24a)	616.5	423	220; 145	
$SiCl_3(CH_3)$ (24b-d)	576-578	450-458	229; 164	229; 229
$SiCl_2(CH_3)_2$ (24b)	533	465	169	
$SiCl_2(CH_2)_3$ (24e)	533	376	167-241	
$SiCl(CH_3)_3$ (24b)		467		
Si-Cl(a) (this work)		553~600		
Si-Cl-Si(a) (this work)		~293		

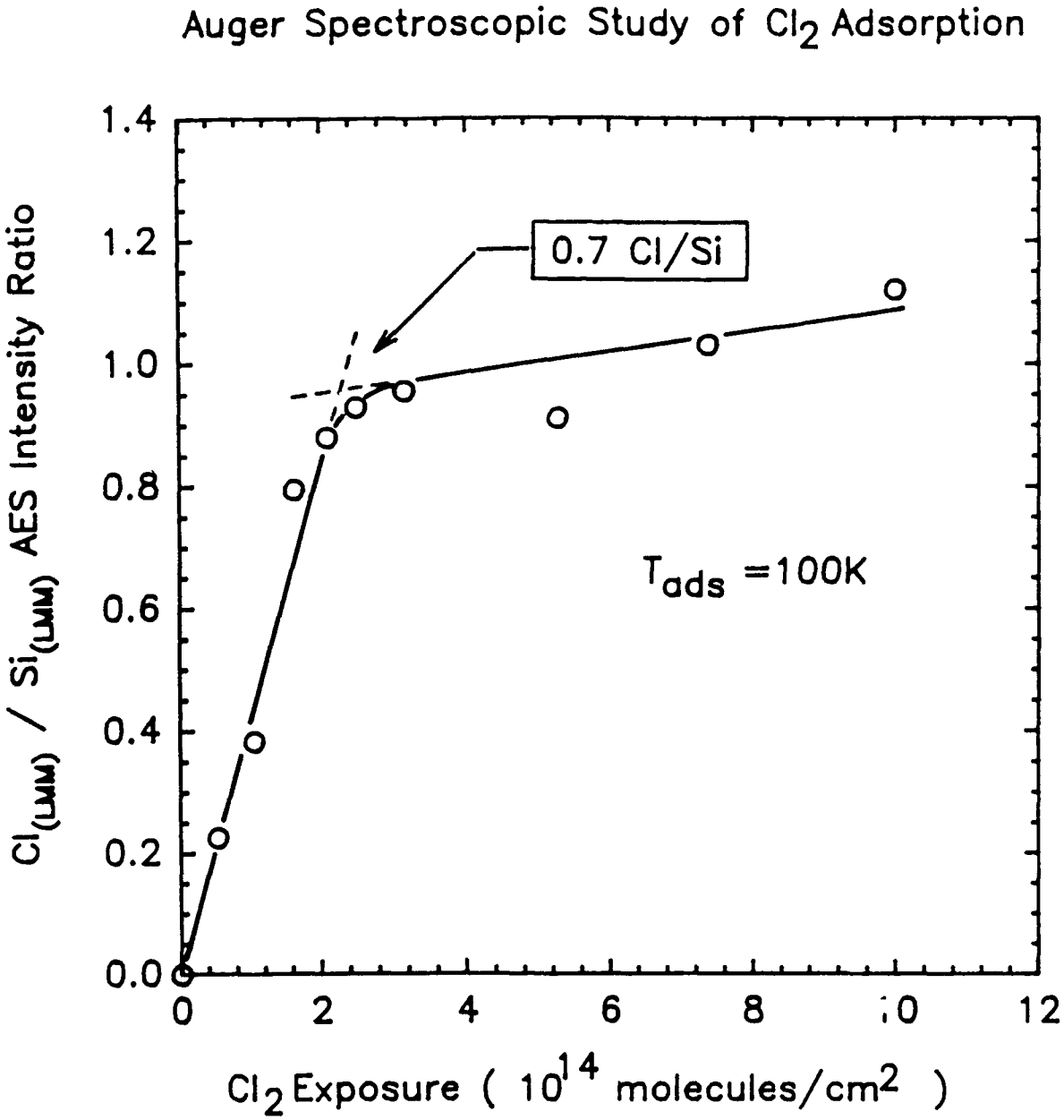

Gao, et.al.,

Figure 1

Gao, et.al,
Figure 2

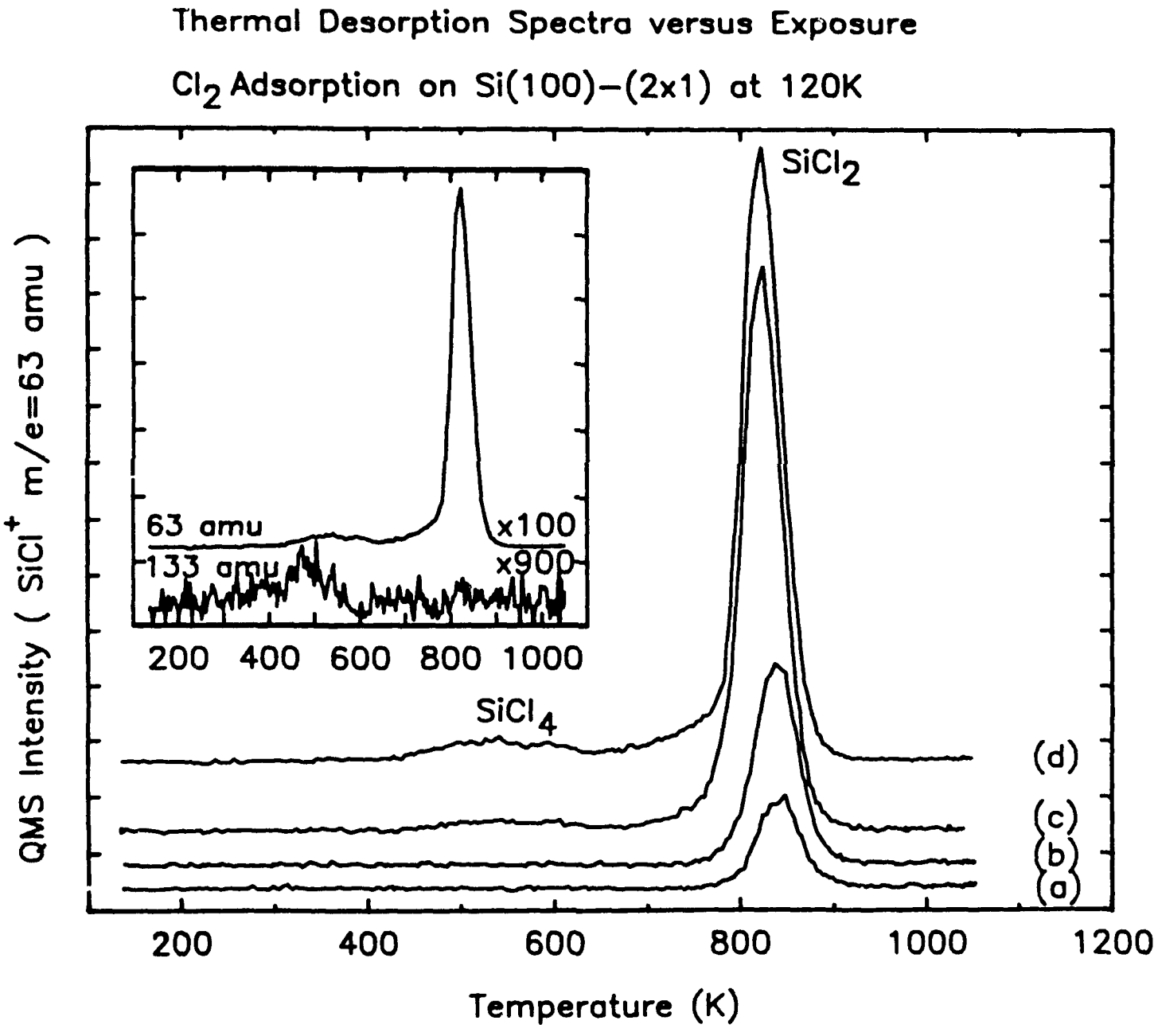

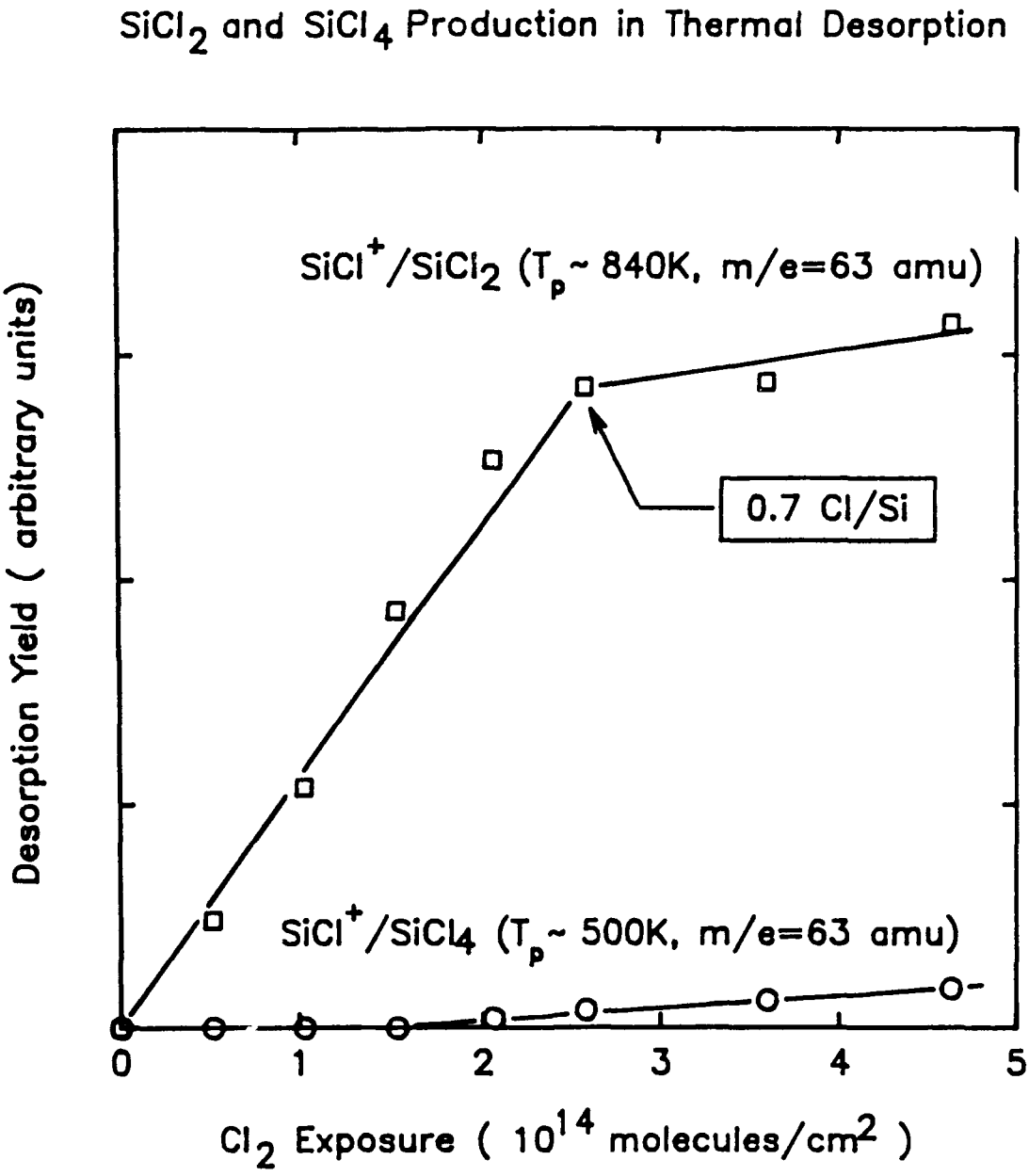

Gao, et.al.,

Figure 3

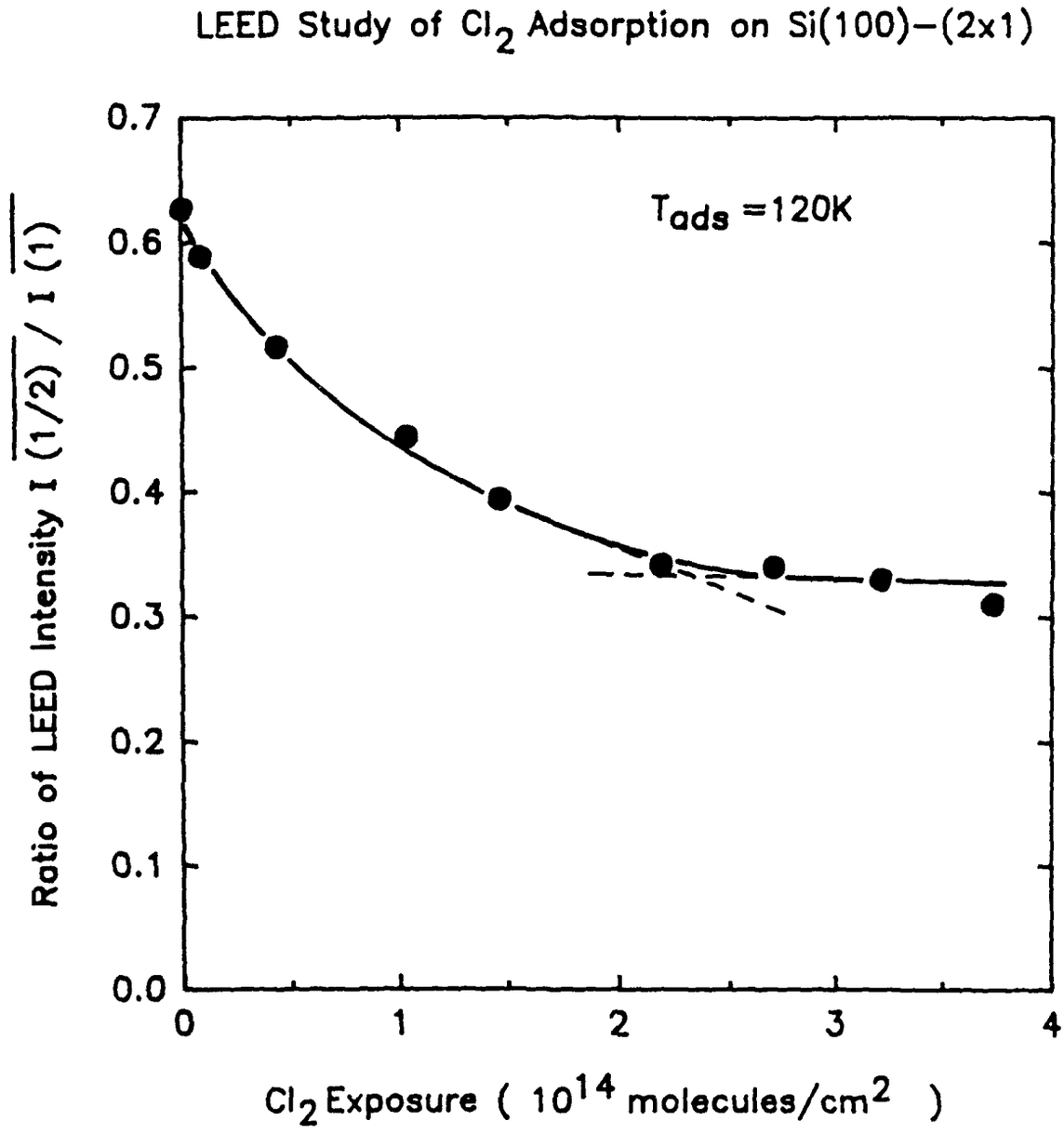

Gao, et.al..

Figure 4

Cl^+ ESDIAD Pattern Development on Si(100) for Increasing Exposure. T = 120 K

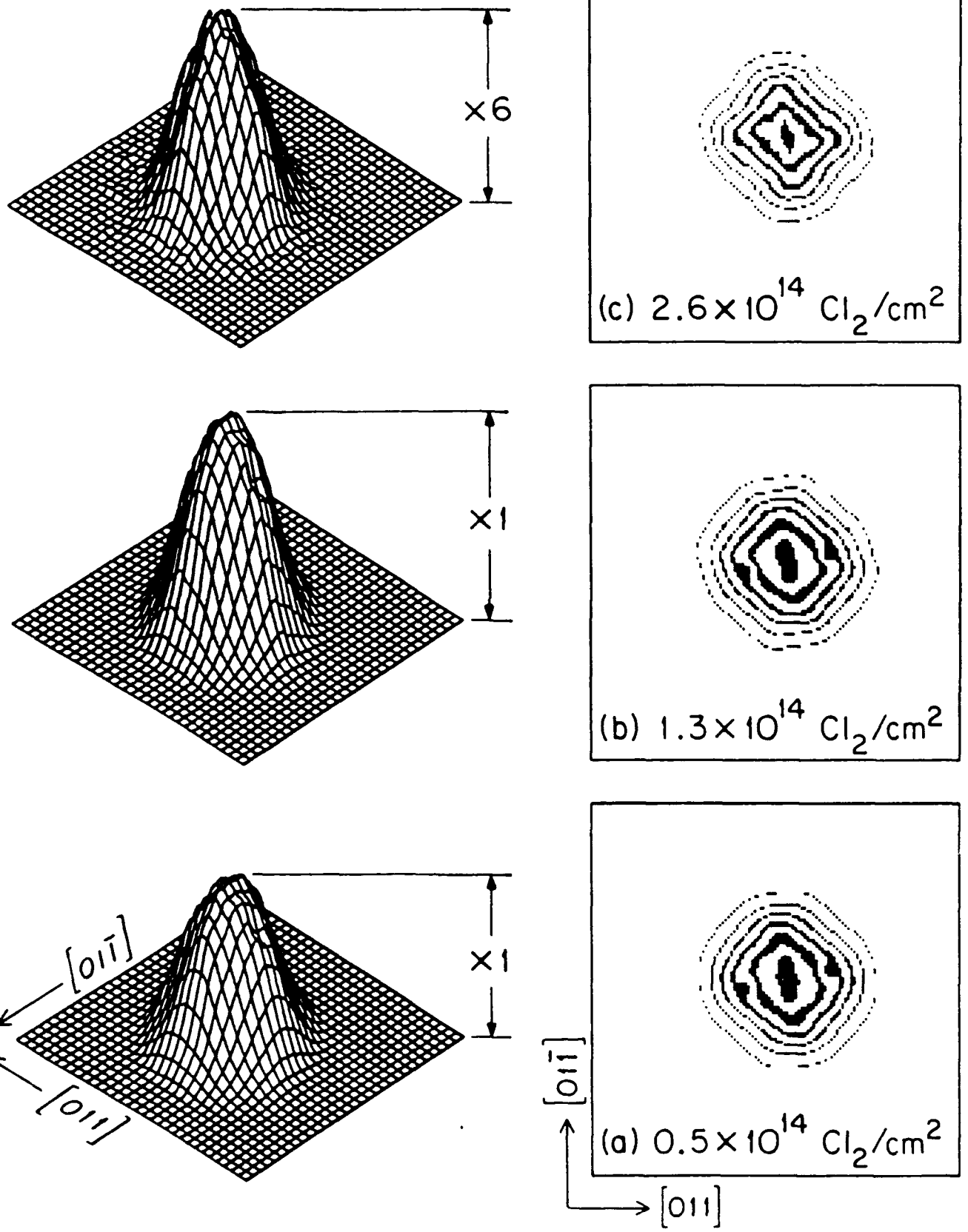

Gao, et.al.,

Figure 5

Cl^+ ESDIAD Pattern Development on Si(100) after Annealing to 673 K. (60 seconds)

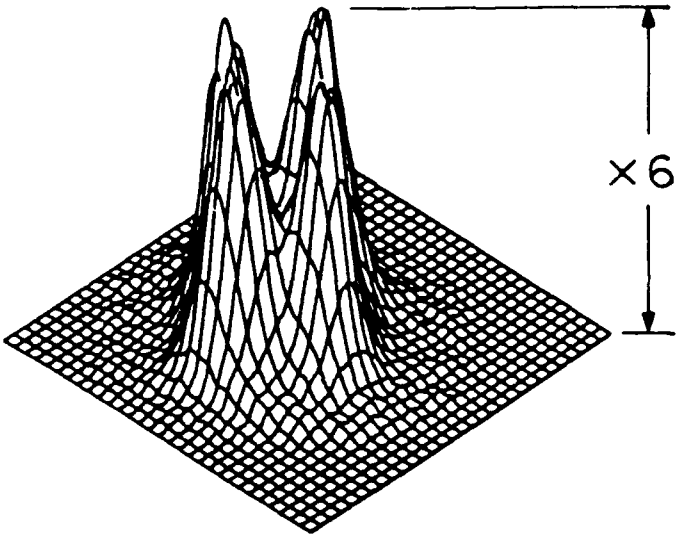

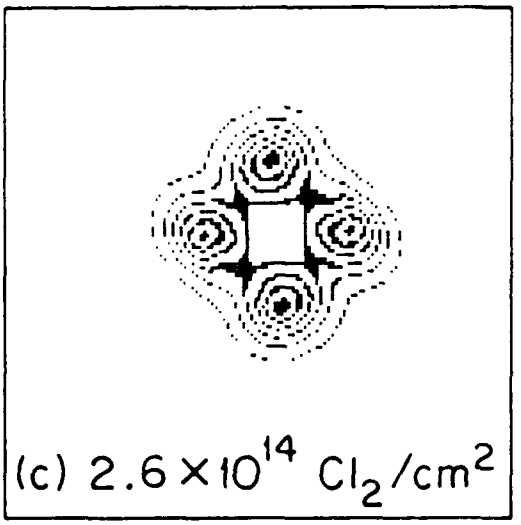

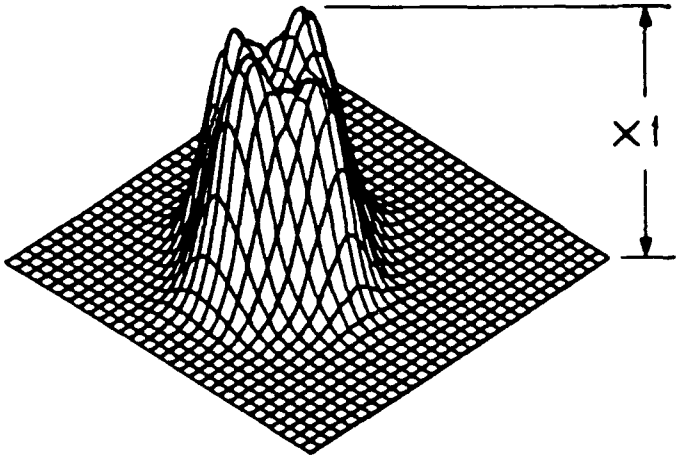

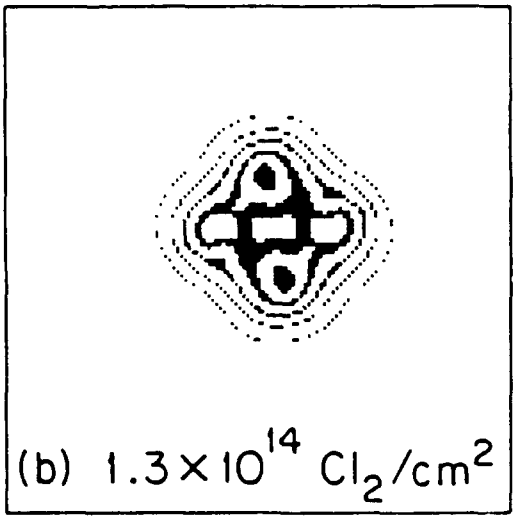

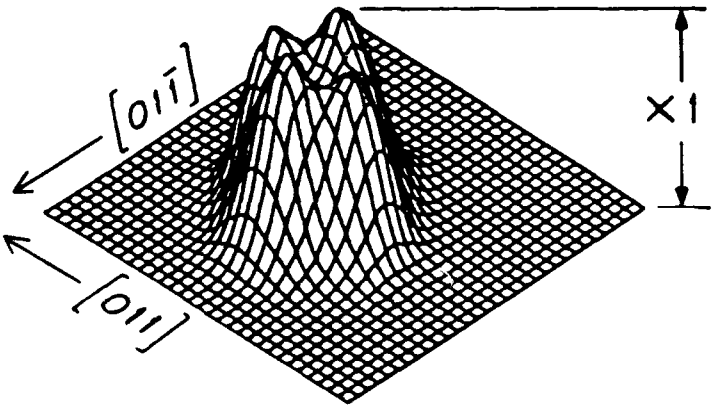

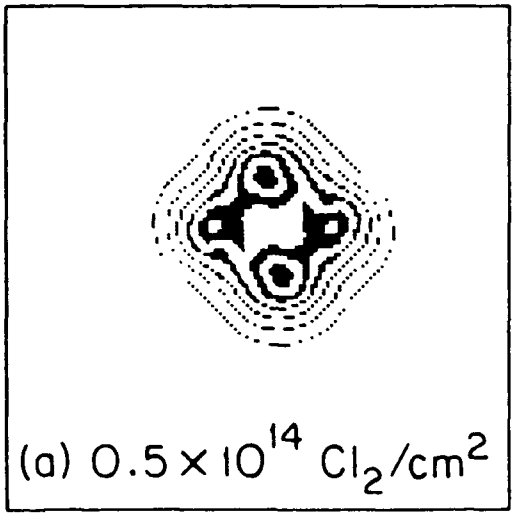

Gao, et.al.,

Figure 6

Thermal Development of Cl^+ ESDIAD Pattern

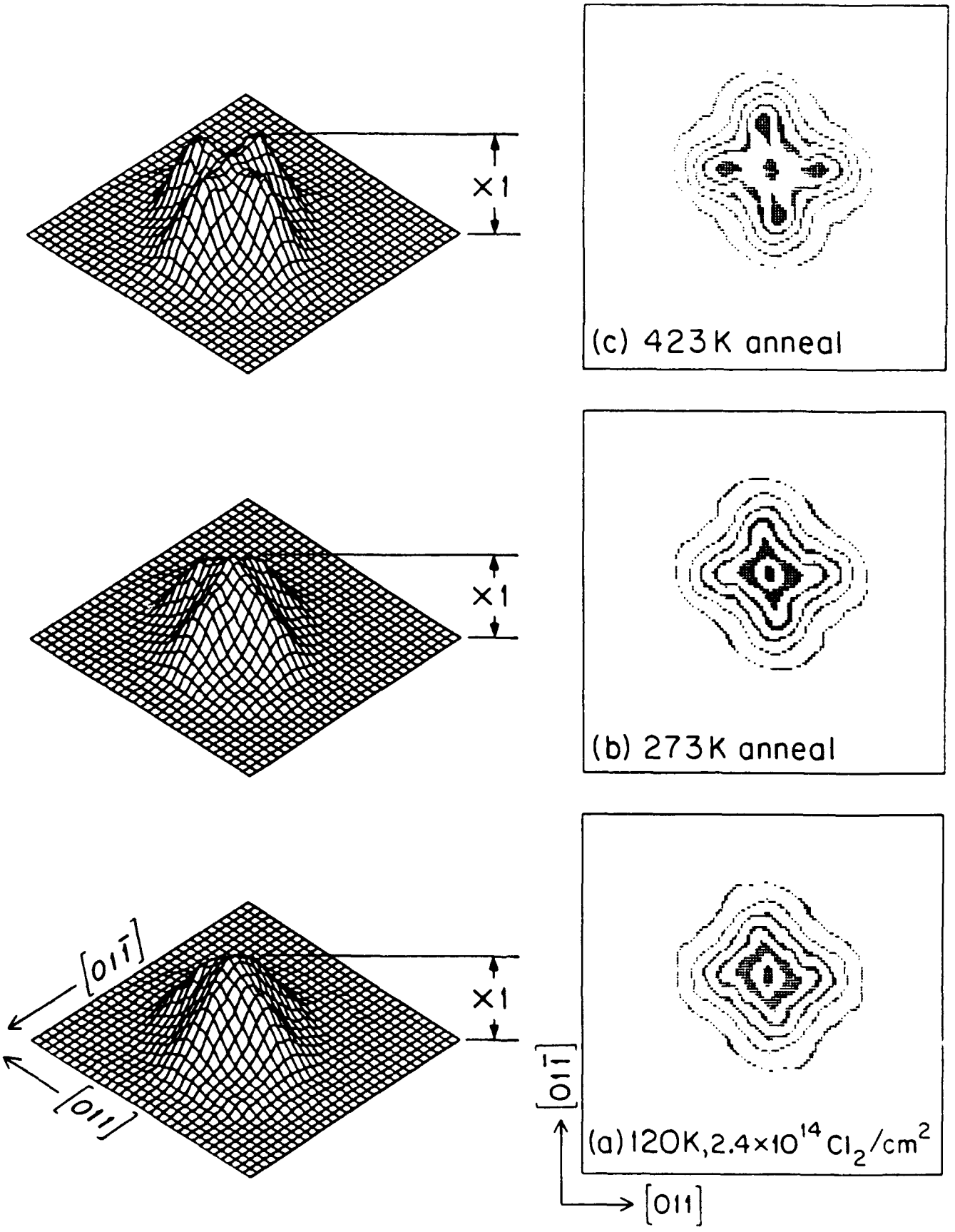

Gao, et.al.,

Figure 7

(a-c)

Thermal Development of Cl^+ ESDIAD Pattern

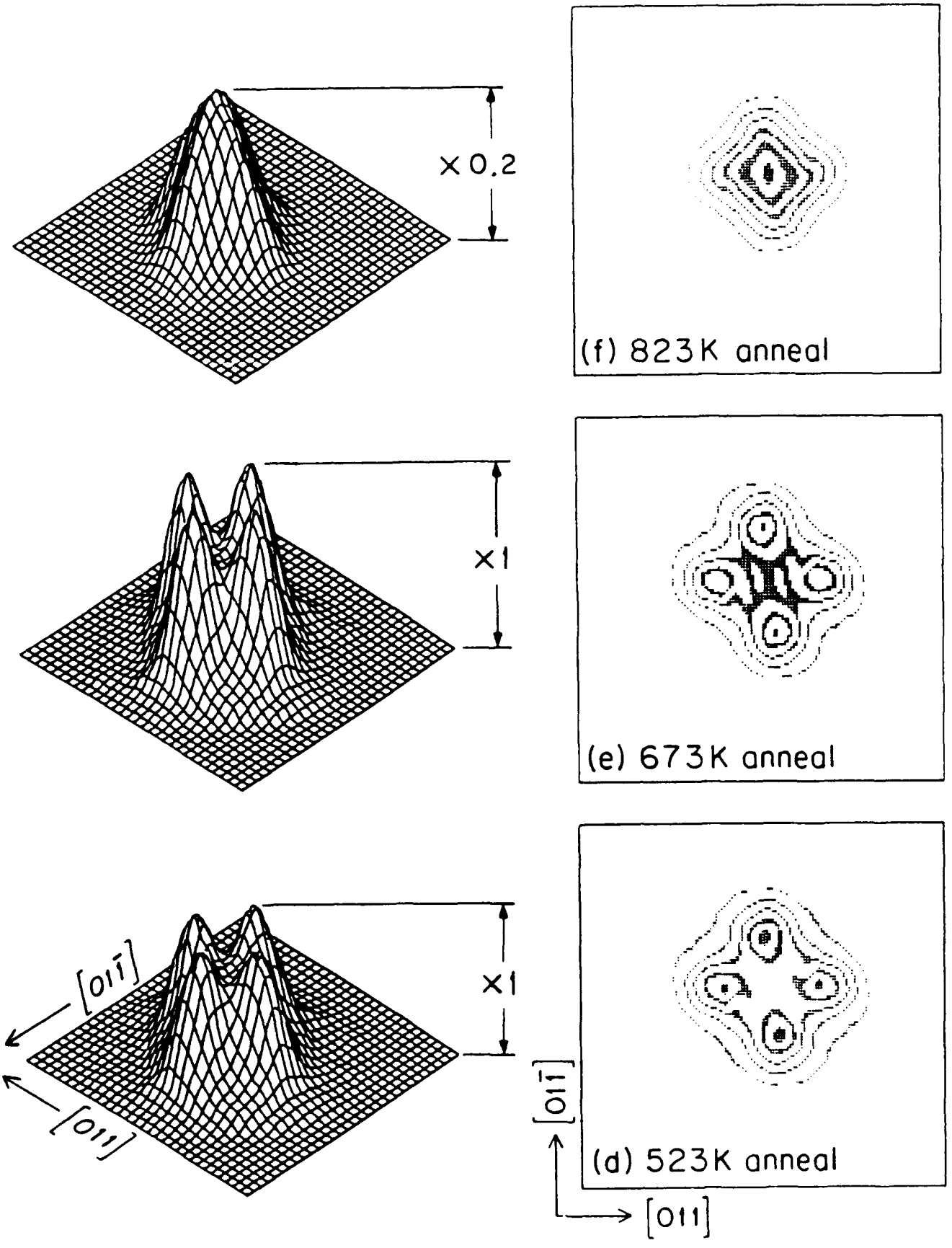

Gao, et.al.

Figure 7
(d-f)

Cross Section View of Thermal Development of Cl^+ ESDIAD Pattern

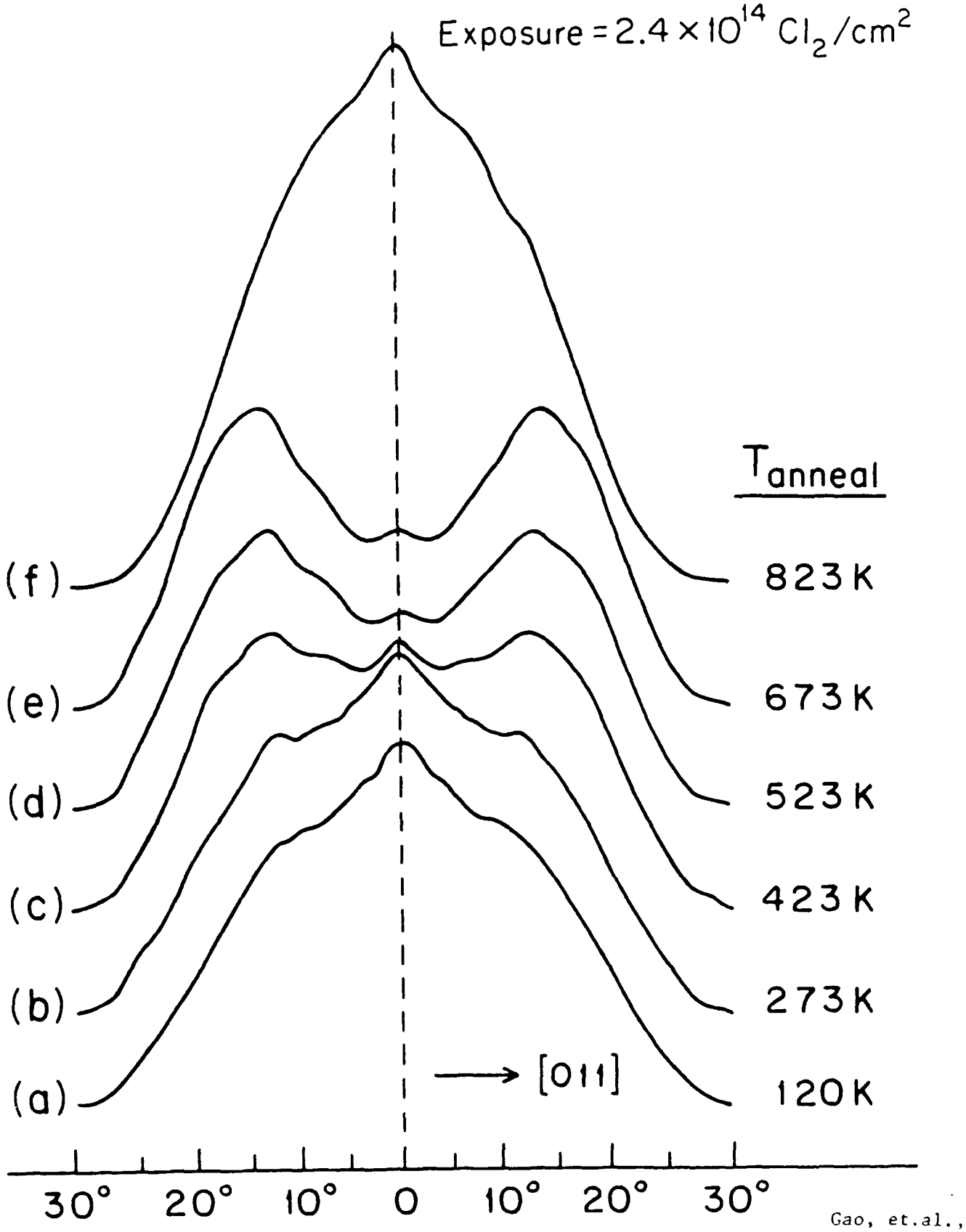

Gao, et.al., Figure 8

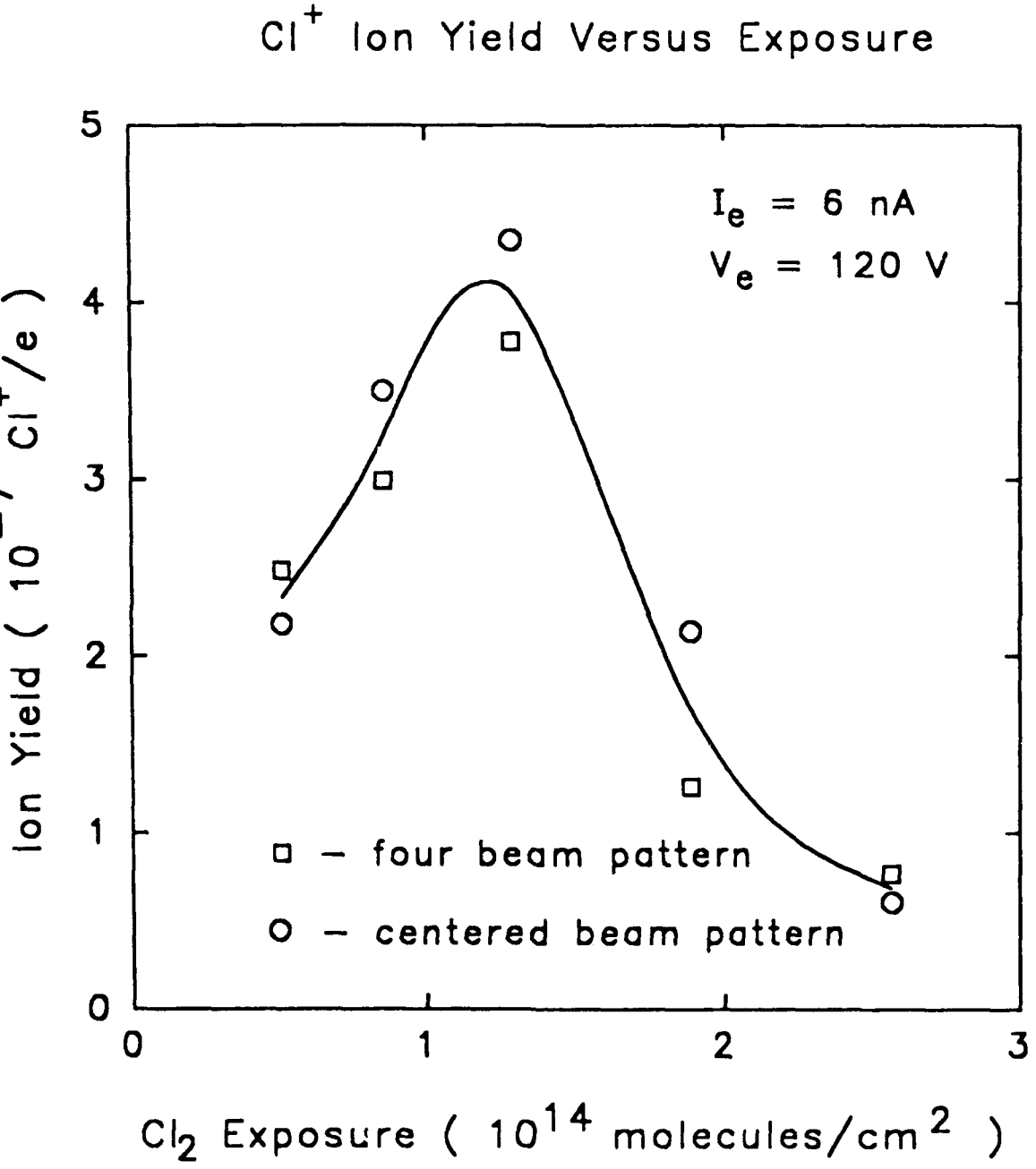

Gao, et.al.

Figure 9

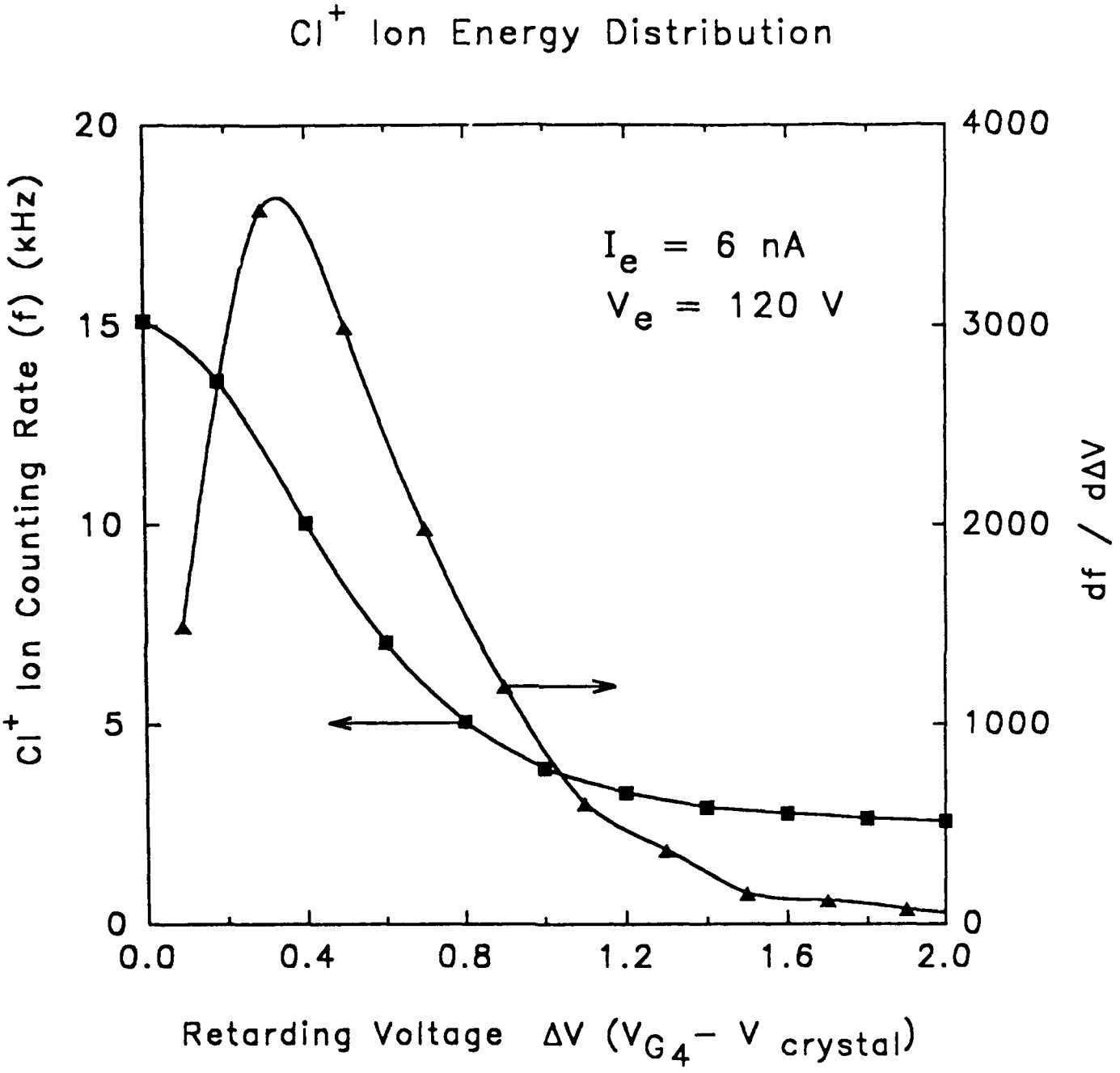

Gao, et.al.

Figure 10

Effect of Heavy Electron Bombardment on Cl Species Adsorbed on Si(100)-(2×1)

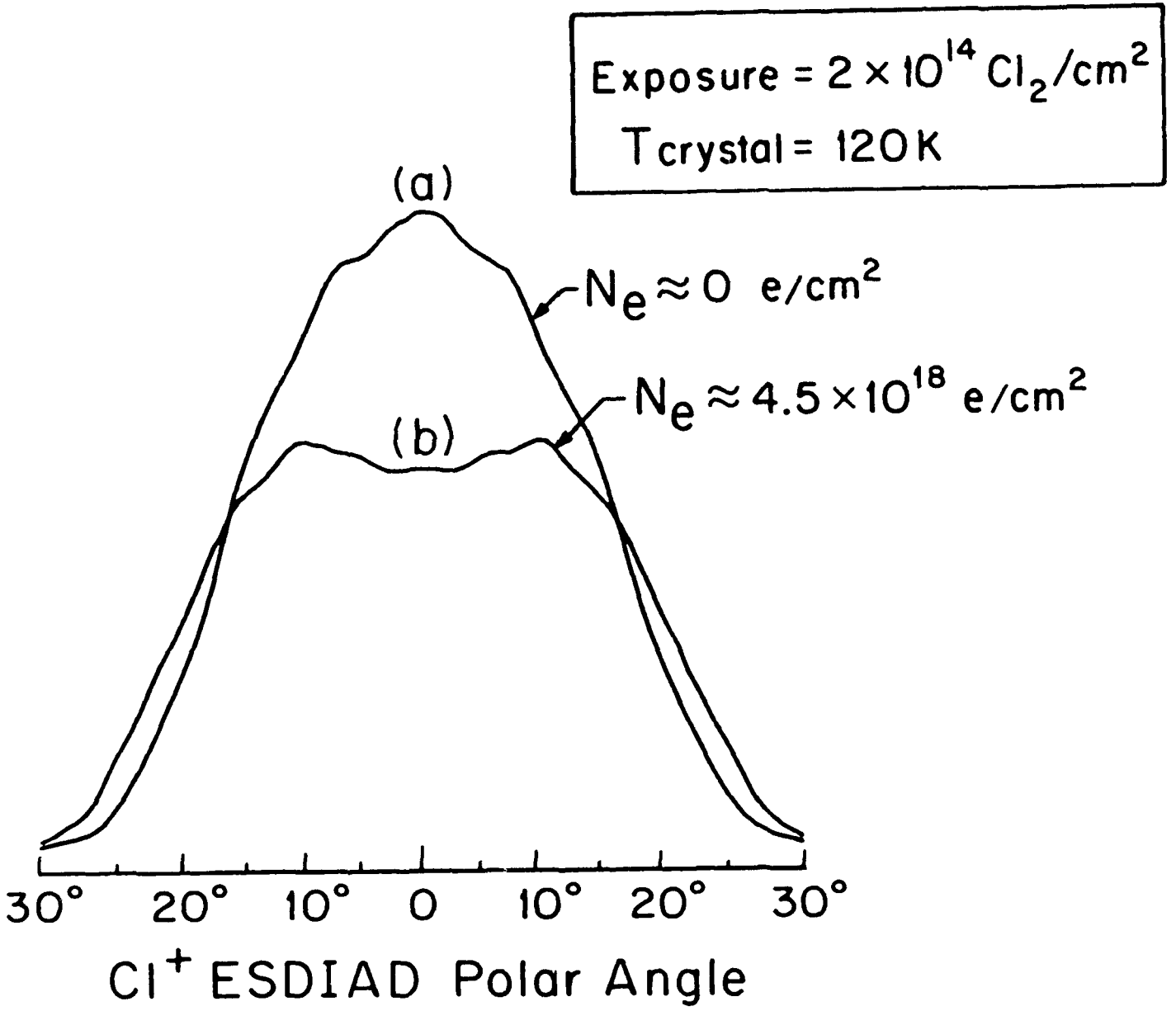

Gao, et.al.

Figure 11

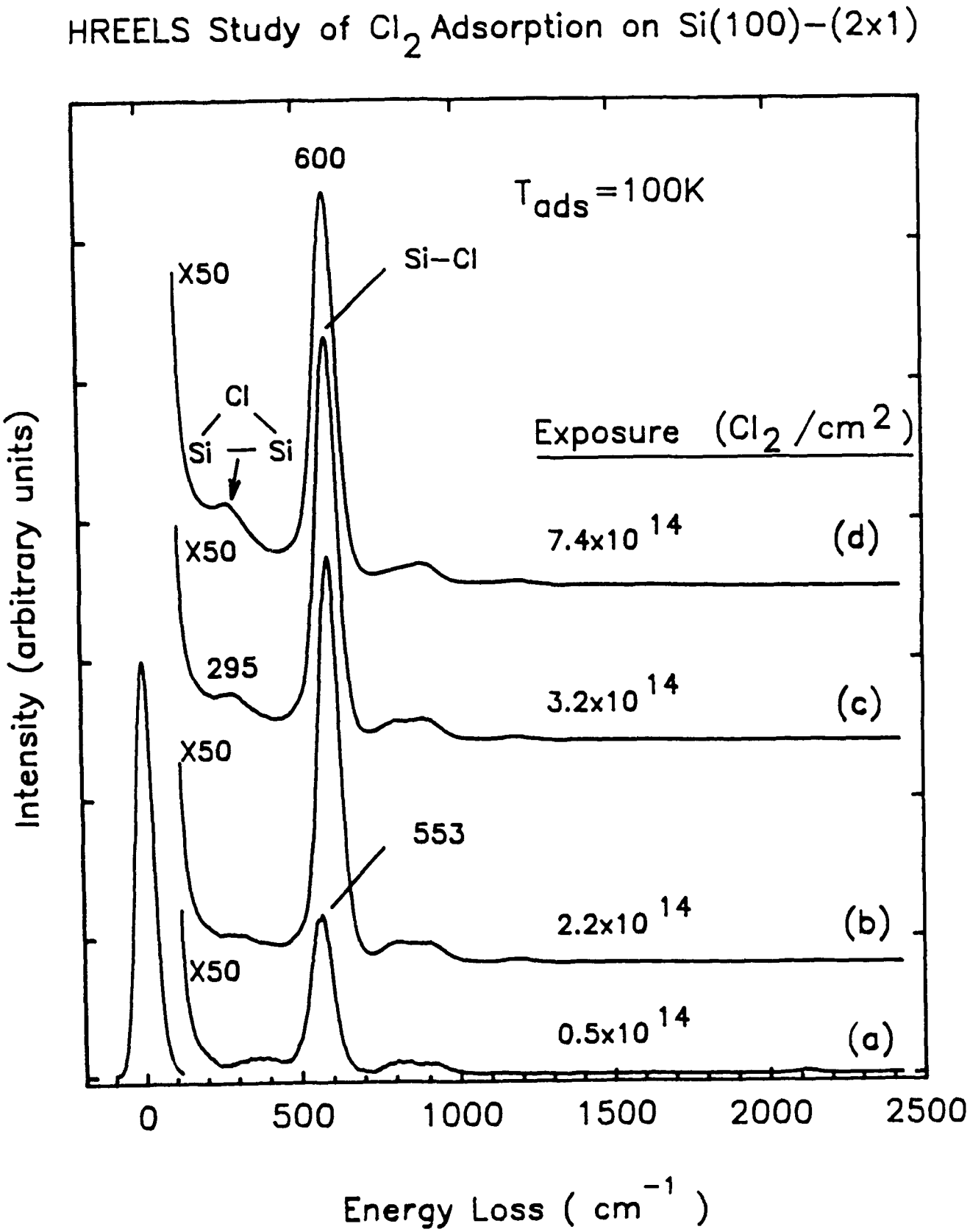

Gao, et.al.,

Figure 12

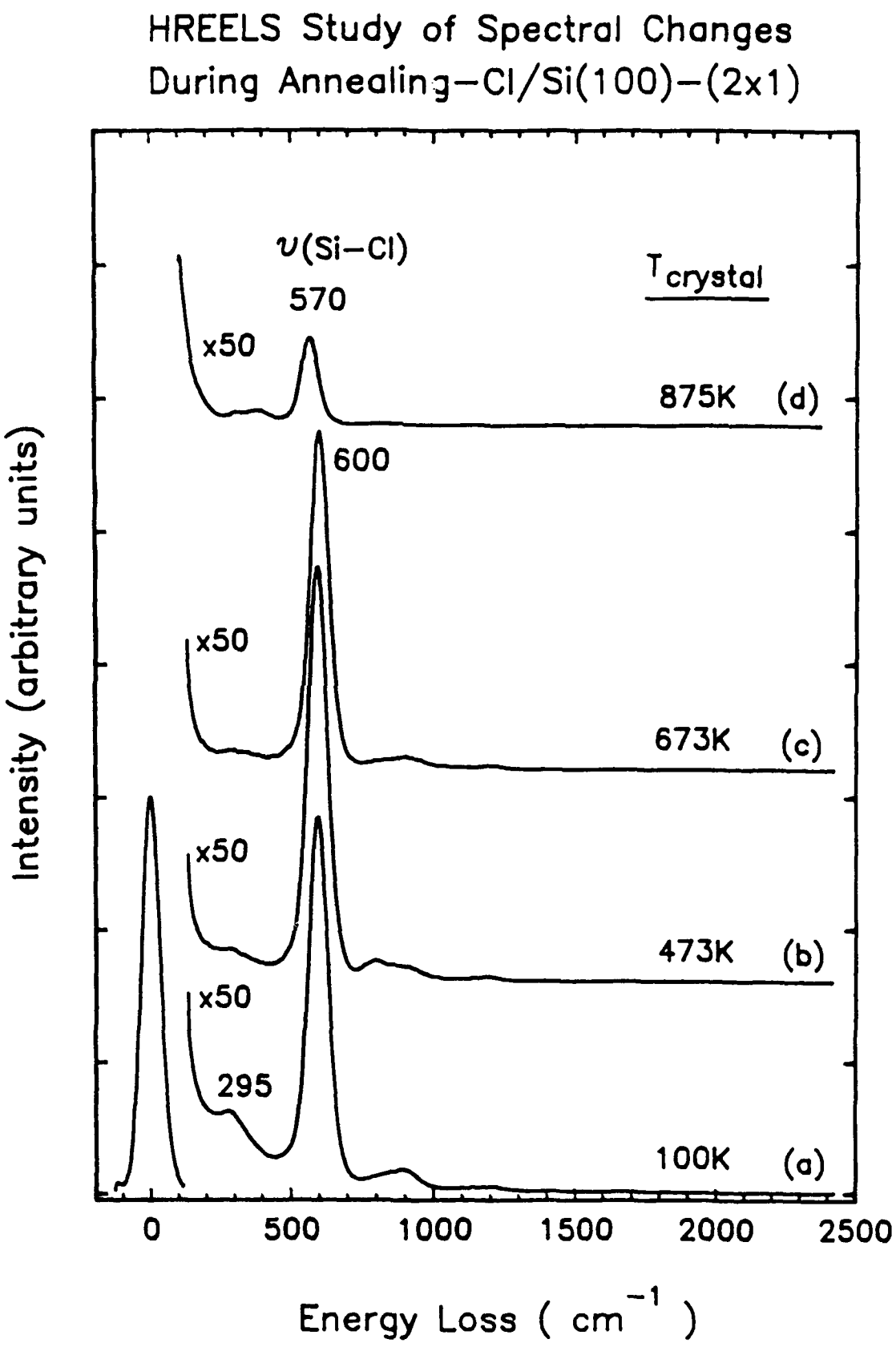

Gao, et.al.,

Figure 13

Gao, et.al.,
Figure 14

Proposed Cl Bonding Configurations on Si(100)-(2x1)

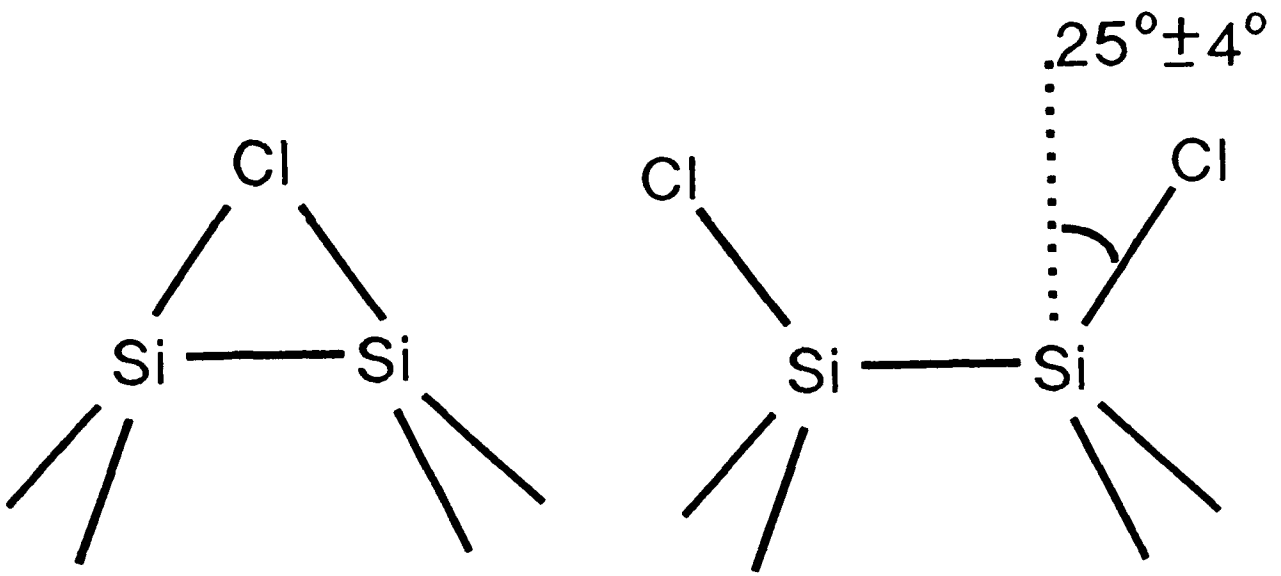

Bridge-bonding Terminal-bonding

Gao, et.al.,

Figure 15

Computer Simulated Ion Trajectories

(a) Crystal Bias Dependence

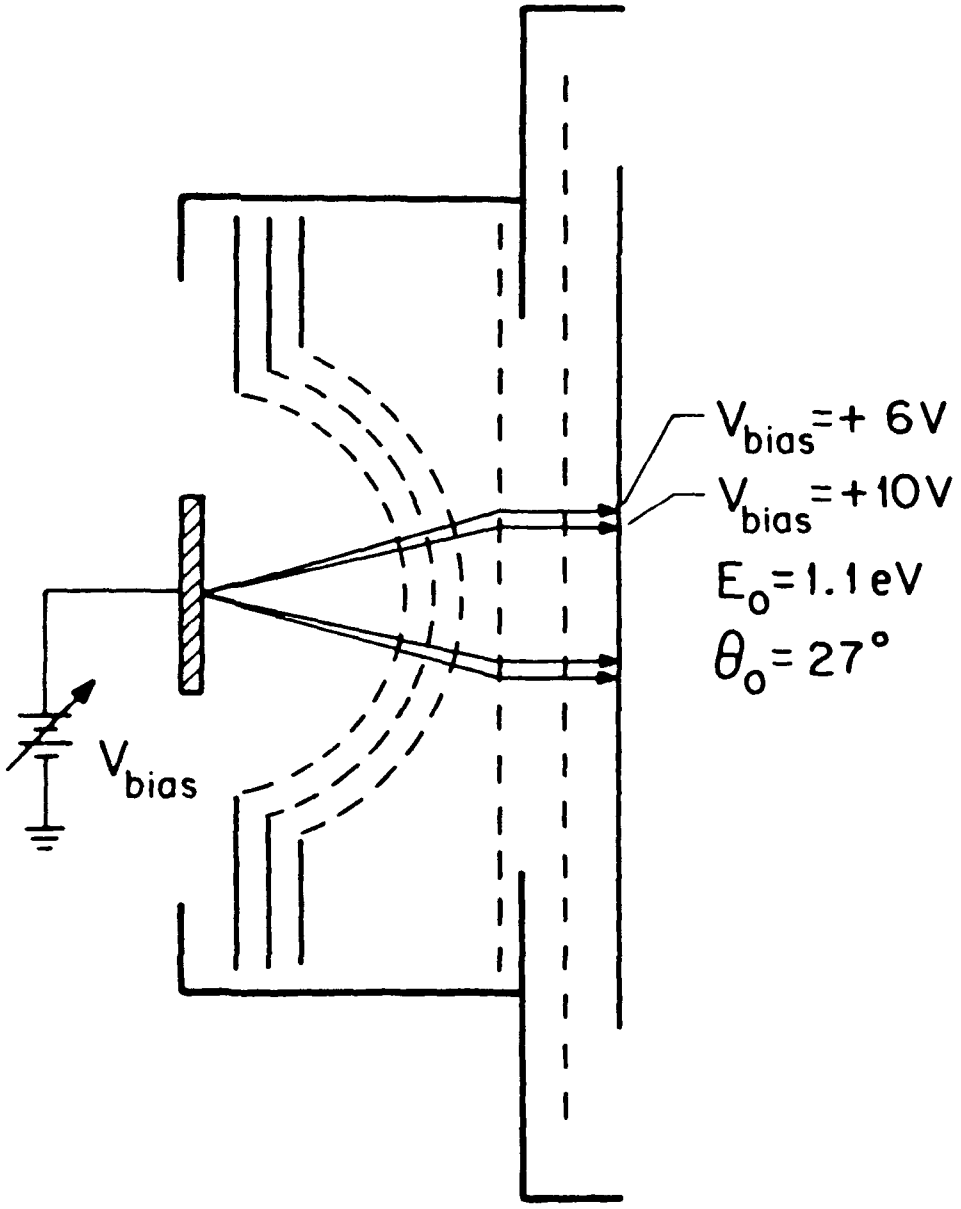

(b) Ion Energy Dependence

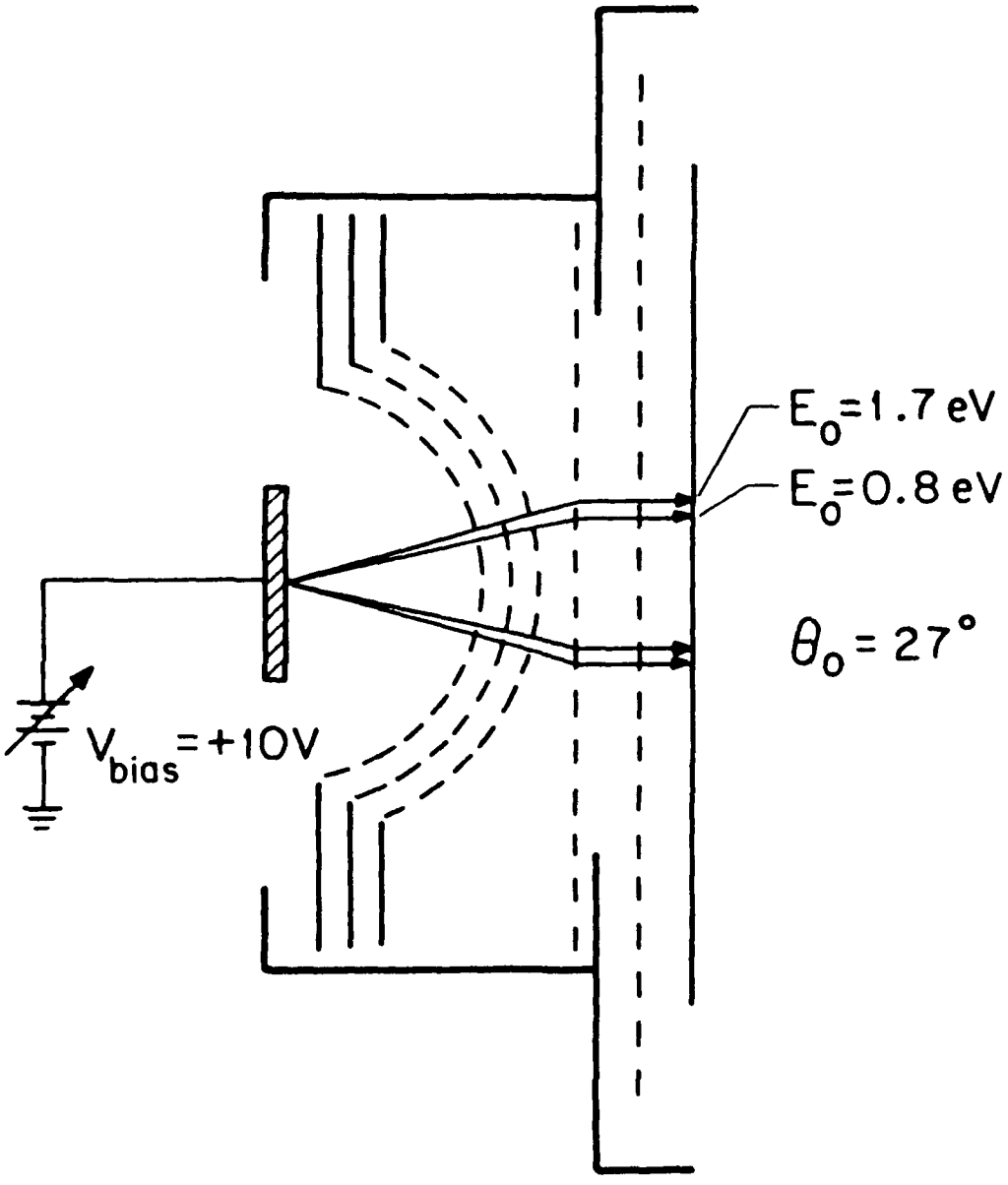

ION ANGLE CORRECTION FOR IMAGE POTENTIAL AND NEUTRALIZATION–O/W (100)

(after Z. Mišković, J. Vukanić and T. E. Madey)

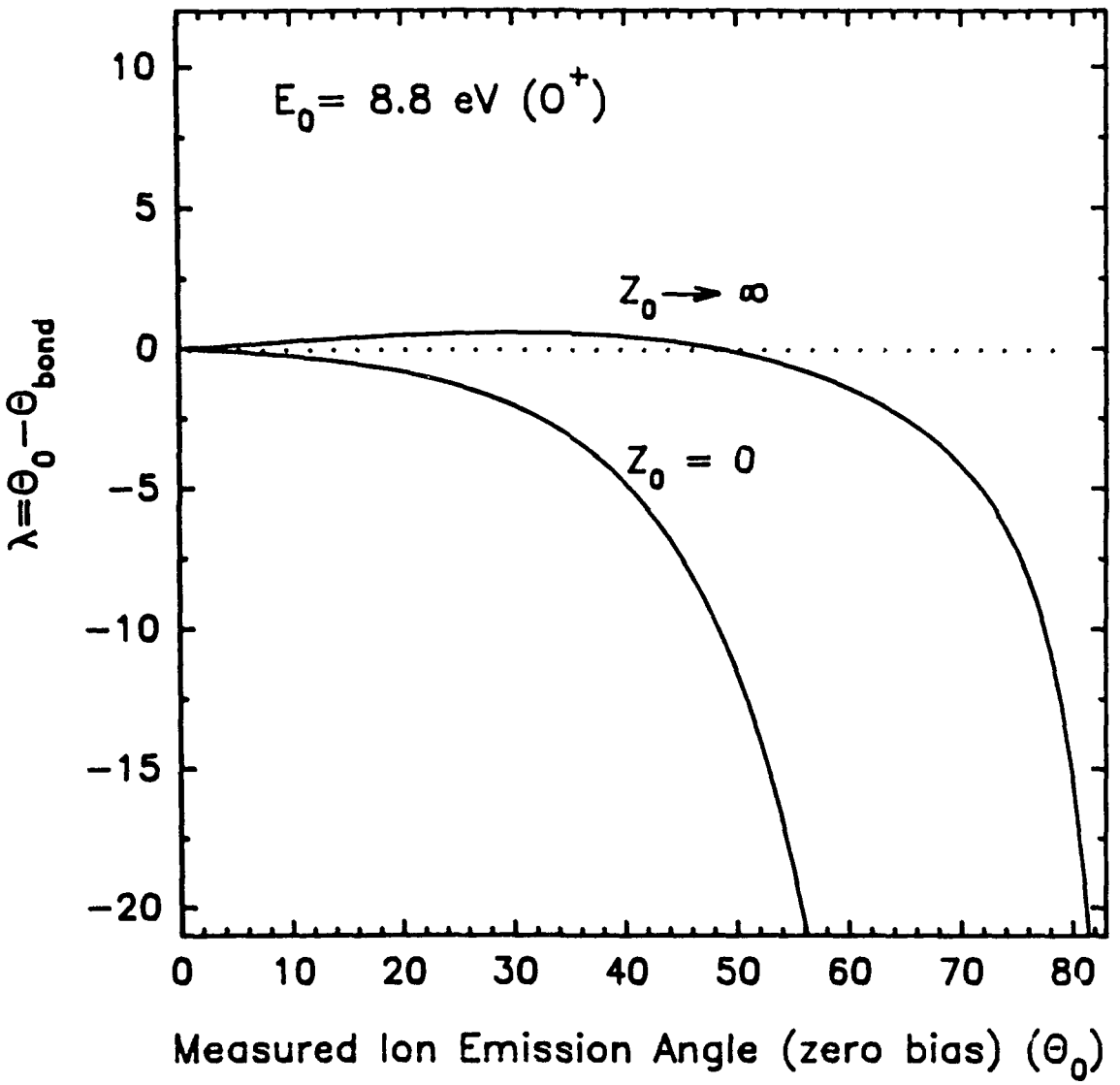

Gao, et.al.

Figure 17

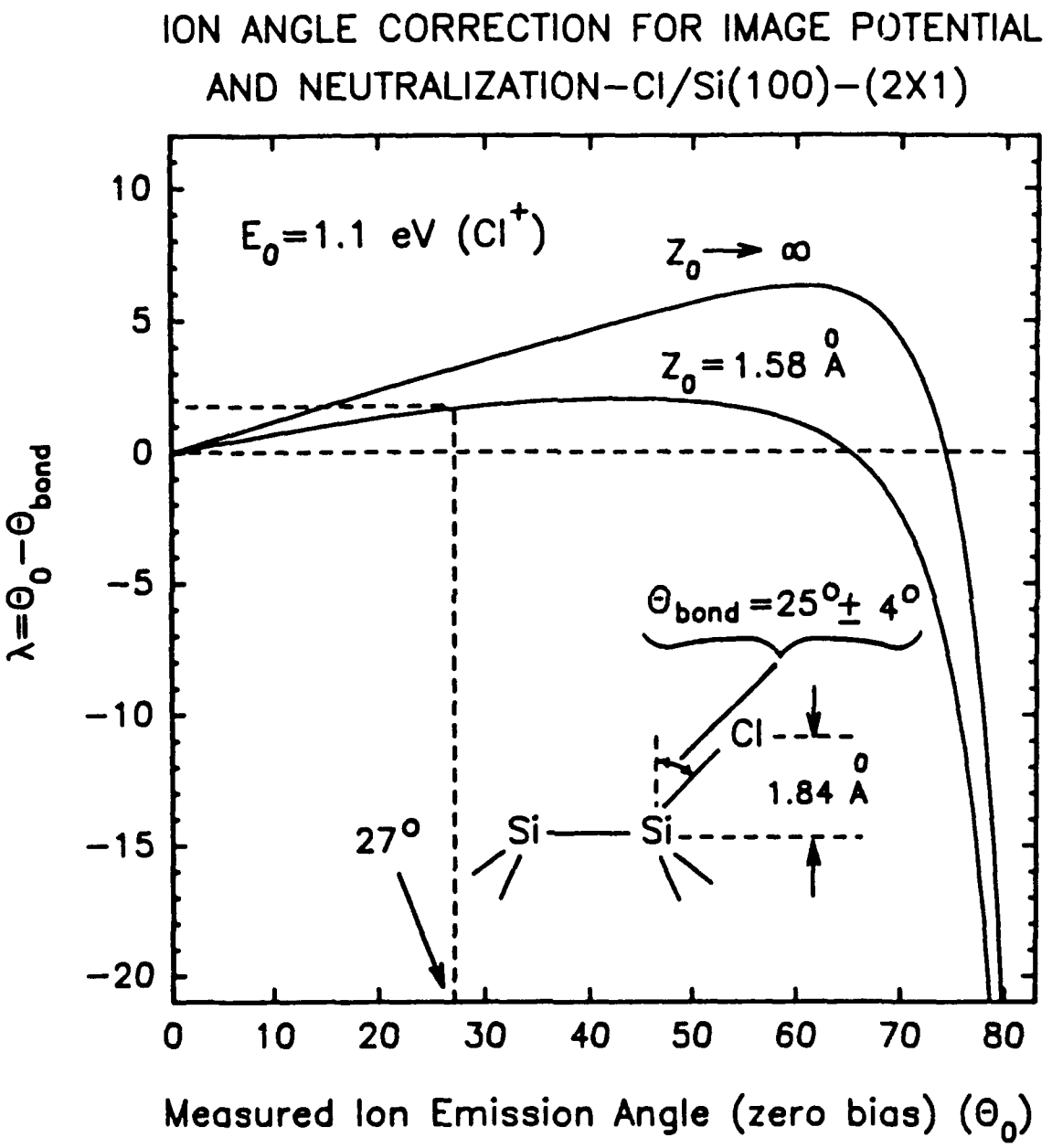

Gao, et.al.

Figure 18

ALE Contractor Distribution List	# Copies
D.T.I.C. Bldg # 5, Cameron Station Alexandria, VA 22314	12
Dr. Andrew Freedman Aerodyne Research, Inc. 45 Manning Road Billerica, MA 01821 Tel: (508) 663-9500 FAX: (508) 663-4918 e-mail: aerodyn@mitvma.mit.edu	1
Dr. Asif Kahn APA Optics 2950 NE 84th Lane Blaine, MN 55434 Tel: (612) 784-4995 FAX: (612) 784-2038 e-mail: 70702.2032@compuserve.com	1
Dr. Duncan Brown Advanced Technology Materials, Inc 7 Commerce Drive Danbury, CT 06810 Tel: (203) 794-1100 FAX: (203) 792-8040	1
Dr. Peter Norris EMCORE Corp. 35 Elizabeth Ave. Somerset, NJ 08873 Tel: (201) 271-9090	1
Prof. Joe Greene Dept. of Materials Science and Engineering University of Illinois 1101 W. Springfield Ave. Urbana, IL 61801 Tel: (217) 333-0747	1
Dr. T. P. Smith IBM T.J. Watson Research Center P. O. Box 218, Route 134 Yorktown Heights, NY 10598 e-mail: trey@ibm com	1
Prof. Robert F. Davis N.C.S.U. Box 7907	1

Raleigh, NC 27695-7907
Tel: (919) 515-2377/3272
FAX: (919) 515-3419
e-mail: davis@mte.ncsu.edu

Prof. Salah Bedair 1
Department of Electrical Engineering
N.C.S.U.; Box
Raleigh, NC 27695
Tel: (919) 515-2336
e-mail: jll@@ecegrad.ncsu.edu

Max N. Yoder 1
ONR Code 1114
Arlington, VA 22217
Tel: (703) 696-4218
FAXes (703) 696-2611/3945/5383
e-mail: yoder@charm.isi.edu

Dr. A. M. Goodman 1
ONR, Code 1114
Arlington, VA 22217
Tel: (703) 696-4218
FAXes (703) 696-2611/3945/5383
e-mail: goodman@ocnr-hq.navy.mil

Dr. J. Pazik 1
ONR Code 1113
Arlington, VA 22217
Tel: (703) 696-4410
FAXes (703) 696-2611/3945/5383
e-mail: pazik@ocnr-hq.navy.mil
pazik%estd.decnet@ccf.nrl.navy.mil

Prof. J. T. Yates, Jr. 1
Dept. of Chemistry
Surface Science Ctr.
University of Pittsburgh
Pittsburgh, PA 15260
Tel: (412) 624-8320
FAX: (412) 624-8552
e-mail: yates@vms.cis.pitt.edu

Robert J. Markunas, R.A. Rudder 1
Research Triangle Institute; Box 12194
Research Triangle Park, NC 27709-2194
Tel: (919) 541-6153
FAX: (919) 541-6515
e-mail: rjmk@rti.rti.org

Professor Mark P. D'Evelyn 1
William Marsh Rice University
Dept. of Chemistry
P.O. Box 1892
Houston, TX 77251
Tel: (713) 527-8101, ext. 3468
FAX: (713) 285-5155
e-mail: mpdev@@langmuir.rice.edu

Dr. Howard K. Schmidt 1
Schmidt Instruments, Inc.
2476 Bolsover, Suite 234
Houston, TX 770054
Tel: (713) 529-9040

FAX: (713) 529-1147
e-mail: hksionwk@ricevm1.rice.edu

Prof. A. F. Tasch 1
Dept. of Electrical Engr. & Computer Science
Engineering Science Bldg.
University of Texas at Austin
Austin, TX 78712
Tel:
FAX:
e-mail: tasch@roz.ece.utexas.edu

Prof. Charles Tu 1
Dept of Electrical & Computer Engr.
UCSD
LaJolla, CA
Tel: (619) 534-4687
FAX: (619) 534-2486
e-mail: cwt@celece.ucsd.edu

Prof. John E. Crowell 1
Department of Chemistry
University of California at San Diego
LaJolla, CA
Tel: (619) 534-5441
FAX: (619) 534-0058
email: jcrowell@ucsd.edu

Prof. P. Daniel Dapkus 1
University of Southern California
University Park
Los Angeles, CA 90089-1147
e-mail: dapkus@mizar.usc.edu
Tel: (213) 740-4414
FAX: (213) 740-8684

Unless you are a small business invoking your 2 year proprietory rights clause, you MUST state on the front page of your report: Approved for Public Release; distribution unlimited.